

1 **Wind and Phytoplankton Dynamics Drive Seasonal and Short-Term**
2 **Variability of Suspended Matter in a Tidal Basin**

3 **Gaziza Konyssova^{1,2*}, Vera Sidorenko^{1,2}, Alexey Androsov^{1,2}, Sabine Horn², Sara Rubinetti^{1,3},**
4 **Ivan Kuznetsov¹, Karen Helen Wiltshire^{2,4}, Justus van Beusekom^{2,5}**

5 ¹ Alfred-Wegener-Institut Helmholtz-Zentrum für Polar- und Meeresforschung, Bremerhaven, Germany
6 ² Wadden Sea Station Sylt, Alfred-Wegener-Institut Helmholtz-Zentrum für Polar- und
7 Meeresforschung, List/Sylt, Germany
8 ³ Dipartimento per lo Sviluppo Sostenibile e la Transizione Ecologica, University of Piemonte
9 Orientale, Vercelli, Italy
10 ⁴ Climate Science Trinity College Dublin, Dublin, Ireland
11 ⁵ Institute for Carbon Cycles, Helmholtz Centre Hereon, Geesthacht, Germany

12 *** Correspondence:**
13 Gaziza Konyssova
14 gaziza.konyssova@awi.de
15 ORCID: 0009-0008-5460-4754

16 **Abstract**
17 Suspended particulate matter (SPM) is a key component of coastal ecosystems, modulating light
18 availability, nutrient transport, and food web dynamics. Its variability is driven by a combination of
19 physical and biological processes that interact across temporal and spatial scales. Using the Sylt-Rømø
20 Bight as a natural laboratory and focusing on the period 2000-2019, in this study, we integrate statistical
21 analysis of observational data from the Sylt Roads monitoring program and local meteorological
22 stations, neural network modelling and Lagrangian transport simulations. This multi-method approach
23 enables us to disentangle and quantify the relative roles of tidal and wind forcing, as well as biological
24 processes in shaping SPM concentrations across various time scales, based on near-surface
25 measurements at two monitoring stations.
26 The findings show that wind intensity dominates short-term SPM variability, particularly at the shallow
27 station, where SPM responds rapidly to local wind-induced resuspension. At the deep station, the wind
28 effects appear with a delay of ~5 days, aligning with tidally induced transport timescales (~133 hours)
29 from shallower resuspension zones, as revealed by Lagrangian simulations. Seasonal patterns are
30 further modulated by both reduced wind intensities and the onset of biological processes, such as
31 phytoplankton blooms, which promote flocculation and subsequent settling in spring and summer.
32 Neural network experiments highlight the shifting seasonal balance between physical and biological
33 controls, The median concentration of SPM decreased by up to 80% from winter to summer.
34 Approximately 40% of this seasonal difference can be attributed to weaker wind conditions, while the
35 remaining ~40% is likely driven by biologically mediated sinking processes.

Deleted: s
Deleted: a long-term biogeochemical time series
Deleted: observations
Deleted: with
Deleted: and neural network modelling
Deleted: dynamics,
Deleted: s
Deleted: and
Deleted: phytoplankton mediated
Deleted: measured
Deleted: near the water surface
Deleted: with
Deleted: ing
Deleted: : models trained on winter data overestimate summer SPM levels by up to 80%, with only ~40% of this discrepancy explained by weaker winds and the remainder likely reflecting biologically mediated sinking processes

53 **1 Introduction**

54 Suspended particulate matter (SPM) is a key component of coastal systems, influencing a wide range of
55 physical and ecological processes. It consists of a mixture of small solid particles of both organic and
56 inorganic origin suspended in the water column with concentrations, size (Eisma, 1986) and
57 composition varying spatially and temporally (Schartau et al., 2019). The spatiotemporal variation in
58 SPM concentrations is driven by an interplay of hydrodynamic, meteorological, and biological factors,
59 which in turn, regulate nutrient availability, light penetration, and organic matter distribution. This
60 directly impacts ecosystem productivity, including the timing of the phytoplankton bloom in spring
61 (Cadée, 1986) and spatial gradients in primary productivity (Cloern, 1987; Colijn, 1982), and trophic
62 interactions (Dolch and Reise, 2010; Graf and Rosenberg, 1997).
63 In tidally energetic environments like the Wadden Sea, the suspended matter gradient is kept upright by
64 the density-driven coastward transport of bottom water and tidal straining (Becherer et al., 2016;
65 Burchard et al., 2008; Flöser et al., 2011). Sediment accumulation is further influenced by
66 hydrodynamic retention mechanisms such as enhanced settling due to the landward dissipation of
67 current velocity, the scour-lag (Dyer, 1995; Friedrichs and Aubrey, 1988) and settling lag effects
68 (Postma, 1967), and the tidal asymmetry formed by the presence of non-linear processes within the tidal
69 system (Dronkers, 1986; Fofonova et al., 2019; Friedrichs and Aubrey, 1988; Hagen et al., 2022). The
70 role of tidal currents in the variability of SPM concentrations is found to be significant through transport
71 processes (Bartholomä et al., 2009; Christiansen et al., 2006) as well as sediment erosion under calm
72 and moderate weather conditions (Bartholomä et al., 2009; Lettmann et al., 2009).
73 In addition to tidal contribution, wind stress and wave action are critical in short-term SPM dynamics.
74 Wind-induced resuspension, particularly in shallow coastal areas, causes episodic increases in turbidity
75 (Aarup, 2002; Fettweis et al., 2012). Stronger and more persistent wind forcing during winter maintains
76 higher SPM concentrations, keeping fine sediments in suspension (de Jonge and van Beusekom, 1995;
77 van Beusekom et al., 1999), while calmer conditions in summer enable enhanced settling (Bale et al.,
78 1985; Verney et al., 2009).
79 Beyond physical resuspension and transport mechanisms, biochemical processes also influence SPM
80 concentrations by modulating aggregation, stabilization, and vertical flux of particulate matter (de Jonge
81 and van Beusekom, 1995; van Beusekom and de Jonge, 2002; Verney et al., 2009). For example,
82 flocculation, the aggregation and breakup of particles, is a key mechanism by which biological activity
83 modulates SPM concentrations (Wotton, 2004; Eisma, 1986). Phytoplankton blooms in spring and
84 summer can promote flocculation, leading to enhanced particle settling and reduced SPM
85 concentrations in the water column (de Jonge & van Beusekom, 1995; Schartau et al., 2019). The
86 process is particularly enhanced by the occurrence of extracellular polymeric substances (EPS),
87 including marine gels such as transparent exopolymeric particles (TEPs), but can also occur due to
88 cohesive properties of fine-grained minerals like clays (Passow, 2002; Verney et al., 2009). The size
89 and cohesiveness of these biologically mediated flocs also govern their settling velocities and
90 resuspension thresholds, affecting how quickly particles are redistributed in the water column. Warmer
91 temperatures also accelerate the decomposition of organic matter (OM), which is nearly always present
92 in natural flocs in various forms (detritus, adsorbed OM molecules, and living OM), and may range
93 from a minor to a dominant fraction of total floc mass (Eisma, 1986; Engel and Schartau, 1999). This

Deleted: levels

Deleted: primary production gradients

Deleted: The focus of this study, the Sylt-Rømø Bight, is a tidally energetic basin within the Wadden Sea (southeastern North Sea), characterized by complex bathymetry and extensive intertidal flats.

Deleted: such

Deleted: The import of SPM and organic matter is reflected by the heterotrophic nature of the Wadden Sea, where remineralisation of organic matter is larger than the local primary production (van Beusekom et al., 1999). Fine

Deleted: s

Deleted: in intertidal areas

Deleted: These processes collectively maintain coastal sediment balance and estuarine morphodynamics, contributing to the long-term evolution of tidal flat environments.

Deleted: tidal-driven transport

Deleted: variability

Deleted:

Deleted: (Aarup, 2002)

Deleted: levels

Deleted: ; Schubel, 1974

Deleted: flocculation and

Deleted: (Bale et al., 1985; Fettweis et al., 2012)

Deleted: SPM also interacts dynamically with a range of biogeochemical processes. It influences light penetration, nutrient availability, and food supply for suspension feeders (Cloern, 1987; Postma, 1981), while biological processes in turn regulate the

Deleted: Fettweis and Van den Eynde, 2003

Deleted: of fine

Deleted: into larger, often organic-rich flocs

Moved (insertion) [4]

Moved (insertion) [1]

Deleted: which

Deleted: constitute anywhere

Deleted: ,

27 directly links SPM dynamics to food-web functioning (Wotton, 2004; Engel & Schartau, 1999). In
 28 addition, temperature also affects top-down controls such as zooplankton grazing, which alters SPM
 29 composition by consuming phytoplankton and restructuring organic aggregates.
 30 In the shallow coastal systems, light can reach the seafloor, stimulating benthic algae growth, provided
 31 water clarity allows sufficient light penetration (Loebl et al., 2007). These benthic processes further
 32 influence SPM concentrations through both stabilization and removal mechanisms. While
 33 microphytobenthos, consisting of benthic diatoms and cyanobacteria, produce biofilms that stabilize
 34 sediments and reduce resuspension (Stal, 2010), filter-feeding organisms, such as mussels (*Mytilus*
 35 *edulis*) and oysters (*Magallana gigas*), alter SPM dynamics by removing fine particles from suspension,
 36 affecting both sediment deposition rates and nutrient cycling (Graf and Rosenberg, 1997). Moreover,
 37 excessive nutrient loads can enhance phytoplankton blooms, whose decay products and extracellular
 38 polymeric substances facilitate biomineral floc formation (Passow, 2002; van Beusekom et al., 1999),
 39 which promotes OM sedimentation and alters benthic-pelagic coupling by influencing the availability of
 40 organic matter to both suspension and deposit feeders. These processes collectively shape coastal
 41 sediment dynamics, contributing to the long-term evolution of tidal flat environments.
 42 While hydrodynamic and wind-driven influences on SPM have been extensively studied, their
 43 interaction with biological processes and relative contributions remain incompletely understood, despite
 44 growing interest. By leveraging long-term ecological monitoring data from the Sylt Roads program, this
 45 study aims to quantify the contributions of tidally induced and wind-driven resuspension and transport,
 46 as well as biologically mediated processes, to the spatiotemporal variability of SPM in the Sylt-Rømø
 47 Bight.
 48 This analysis integrates high-resolution in situ measurements from two LTER stations from 2000 to
 49 2019, meteorological data from the station List (Sylt, Germany), and outputs from hydrodynamic and
 50 neural network modelling to evaluate SPM dynamics across short-term (hourly to daily) and seasonal
 51 timescales. The following research questions guide the study: (1) What are the dominant mechanisms
 52 driving SPM variability across different temporal scales? (2) How do these mechanisms differ between
 53 the two monitoring stations within the Sylt-Rømø Bight? (3) How important are biological processes in
 54 shaping observed SPM concentrations?

Moved (insertion) [2]

Deleted: ing

Moved up [1]: The size and cohesiveness of these biologically mediated flocs also govern their settling velocities and resuspension thresholds, affecting how quickly particles are redistributed in the water column.

Moved (insertion) [3]

Deleted: B

Deleted: levels

Deleted: organic

Deleted: , which

Deleted: The combination of wind-driven resuspension and strong tidal currents frequently elevates SPM concentrations, leading to fluctuating turbidity that can impact seagrass (*Zostera spp.*) productivity (Dolch and Reise, 2010).

Deleted: Despite extensive research on

Deleted: understudied

Deleted: By using chlorophyll-a as a proxy for phytoplankton biomass, we approximate biological contributions triggered by phytoplankton to the variability of SPM levels, e.g. through flocculation and sediment stabilization.

Deleted: The study is guided by the following research questions

155 2 Data and Methods

156 2.1 Area Description

157 The investigations were carried out in the Sylt Rømø Bight, a shallow, tidal basin in the northern
 158 Wadden Sea (southeastern North Sea; see Fig. 1). The basin is semi-enclosed due to two causeways at
 159 its northern and southern ends, isolating it from neighboring basins. Its only connection to the North Sea
 160 is through the deep tidal inlet Lister Deep, between the islands of Sylt and Rømø. The bay spans
 161 approximately 410 km² and features a highly variable topography, including extensive intertidal flats
 162 (>45%), shallow subtidal zones (~35%), and deep tidal channels (~10%). The Sylt-Rømø Bight's
 163 bathymetry is characterised by a mean water depth of approximately 4 m, with a maximum depth of
 164 about 37 m observed in the tidal inlet Lister Deep. Most subtidal and ~72% of intertidal sediments are

185 sand-dominated. The basin also features a small sheltered embayment Königshafen, with an average
186 depth of ~2m and large areas becoming exposed at low tides.
187 The tidal range in the bight averages 2 m, based on observations at the List tide gauge (E.U. Copernicus
188 Marine Service Information, doi.org/10.48670/moi-00036). Tidal forcing accounts for over 80% of
189 depth-averaged velocity variability under regular wind conditions, in the absence of storms, and over
190 90% during spring tides (Fofonova et al., 2019). The bight receives minimal fluvial input, with small
191 rivers such as the Vidå and Brede Å (see Fig.1), contributing only 4–10 m³/s of freshwater (Purkiani et
192 al., 2015). Water exchange with the open North Sea occurs exclusively through Lister Deep, a 2.8 km
193 wide tidal inlet. At the mouth of Lister Deep, a prominent ebb-tidal delta extends seaward, acting as
194 both a sediment trap and a pathway for sediment redistribution within the bight (Dissanayake et al.,
195 2012). Localized anthropogenic disturbance may also influence sediment availability and distribution in
196 the region, although detailed records of maritime traffic, dredging operations, and benthic trawling
197 specific to the Sylt-Rømø Bight are limited. However, studies from the broader Wadden Sea show that
198 anthropogenic activities such as bottom trawling (e.g., Bruns et al., 2023; Depestele et al., 2016),
199 dredging (de Jonge and de Jong, 2002; de Jonge, 1983; van Maren et al., 2015), and mussel farming
200 (Jansen et al., 2023) are recognized drivers of sediment disturbance and resuspension.

Deleted: (

Deleted: D

Deleted: D

Deleted: V

Sylt-Rømø Bight

Legend

- tidal flats
- bivalve beds
- seagrass
- salt marshes

- Water depth
- >1-2 m
 - >2-5 m
 - >5-10 m
 - >10-20 m
 - >20 m

- tide gauge stations
- LTER sampling stations



Figure 1: Map of the Sylt-Rømø Bight showing bathymetry, key habitats (tidal flats, bivalve beds, seagrass meadows, and salt marshes), LTER sampling stations (Deep Station – Lister Ley; Shallow Station – Königshafen), tide gauge locations (List, Havneby, Vidå), and rivers (Brede Å and Vidå). The basin is connected to the North Sea via the tidal inlet Lister Deep and laterally enclosed by causeways to the north and south.

Deleted: A notable feature is Königshafen – a small shallow embayment at the northern tip of the island of Sylt. The embayment is sheltered from winds and waves, and experiences semidiurnal tides with amplitudes reaching 1.7 m (Kristensen et al., 2000; Reise and Siebert, 1994). With an average depth of ~2 m, large areas become exposed at low tide.

216 2.2 FESOM-C Model

217 This study used the coastal hydrodynamic model FESOM-C (Androsov et al., 2019). FESOM-C is
218 designed explicitly for high-resolution coastal applications and employs a finite-volume cell-vertex
219 discretization on unstructured meshes composed of triangles and quadrilaterals. This allows for flexible
220 spatial resolution down to several metres, suitable for simulating complex coastal dynamics (Fofonova
221 et al., 2019; Kuznetsov et al., 2020, 2024; Neder et al., 2022; Sprong et al., 2020; Sidorenko et al.,
222 2025).

Deleted: specifically

223 2.2.1 Model Setup

224 The setup utilized an unstructured hybrid mesh of 208,345 nodes and 211,545 elements. Due to the
225 semi-enclosed state of the bight, the mesh contains a single open boundary at the seaward edge of the
226 domain, connecting the basin with the North Sea. The horizontal spatial resolution varies from up to 2
227 m in wetting-drying zones to 304 m in the deeper outer part (near the open boundary). The experiments
228 were carried out by running 2D barotropic simulations with the wetting/drying option enabled to
229 capture the periodic submergence and exposure of intertidal areas. The model timestep was set to ~ 0.25
230 seconds, with data output every ~20 minutes of simulation time. The bottom friction coefficient was
231 applied as 0.0025, a value identified as optimal in prior studies of the same study area when using
232 TPXO9 tidal solution (Fofonova et al., 2019; Konyssova et al., 2025).

Deleted: .

Deleted: .

233 The simulations are driven by tidal forcing alone, applied at the open boundary. For an accurate
234 simulation of the tidal dynamics, thirteen major tidal harmonic constituents (M2, S2, N2, K2, K1, O1,
235 P1, Q1, Mm, Mf, MN4, 2N, and S1) and two over-harmonics (M4, MS4) were prescribed by their
236 phases and amplitudes at the open boundary based on TPXO9 tidal atlas (Egbert and Erofeeva, 2002).
237 This selection of the tidal solution was justified by its robust performance and is one of the most
238 optimal for the North Sea (Fofonova et al., 2019). The current setup has been validated in a previous
239 work by Konyssova et al. (2025). The model's performance has been validated using tidal gauge (TG)
240 data from stations List, Vidå, and Havneby, displayed in Fig. 1 (performance results are provided in the
241 Supplementary Materials, Table S1). Since the numerical setup remains unchanged, we refer to
242 Konyssova et al. (2025) for full validation details.

Deleted: .

Deleted: the effects of higher harmonics and over-harmonics (e.g., Fofonova et al., 2019; Stanev et al., 2016) were taken into particular consideration as their role in shaping the hydrodynamics in such a shallow intertidal basin is significant. Therefore,

243 2.2.2 Lagrangian Module

244 To assess tidally driven spatial connectivity and transport timescales within the basin, we performed
245 Lagrangian simulations using FESOM-C Drift, a post-processing tool designed for particle tracking.
246 The model advects massless passive particles based on the velocity fields produced by the
247 hydrodynamic model. In this study, we use the term “passive tracers” to denote Lagrangian particles
248 without weight or settling properties. This is equivalent to virtual Lagrangian particles commonly
249 applied in particle tracking studies and should not be confused with dye experiments that represent
250 concentration changes in space and time.
251 The experiment involved releasing passive tracers from all grid elements within the domain that are
252 consistently inundated during every flood phase. We released about 90,000 tracers at three-hour
253 intervals over six weeks (169 iterations in total). Each tracer was tracked for up to three weeks and was

Deleted: . These simulations were carried out

Deleted: It simulates the movement of

Deleted: calculate

Deleted: released

Deleted: every

Deleted:

Deleted: s

269 removed from the simulation once it reached either of the two Sylt Roads sampling stations (see Fig. 1
270 and Section 2.3.1). The iterative release process was designed to capture the full range of tidal
271 conditions and the complexity of hydrodynamic transport within the basin, ensuring that the results are
272 statistically robust. Upon arrival at a station, tracers were immediately removed to prevent post-arrival
273 movements from influencing the mapped source regions and transport pathways. The simulations were
274 conducted independently for each station, focusing exclusively on the paths from the release locations
275 to the respective sampling site. If a tracer did not reach the designated station within the simulation time
276 frame, it was considered to originate from a region that falls outside the station's dominant transport
277 pathways.

278 The first analysis approach assessed the source regions of passive tracers arriving at the sampling
279 stations. This allows us to evaluate the connectivity between different subareas of the basin and the
280 sampling sites. The probability of SPM originating from a given area was mapped based on the
281 cumulative occurrence of tracer pathways across all iterations. Higher probability values indicate areas
282 that more frequently serve as source regions or transport pathways for SPM reaching the sampling
283 stations.

284 The second part of the analysis was conducted to estimate the mean transit time of the tracers reaching
285 the sampling stations from shallow source zones, where resuspension typically occurs (defined here as
286 areas <2 m deep, based on de Jonge & van Beusekom, 1995). The mean transit time over all
287 implementations was calculated for all elements whose tracers reached the stations within the simulated
288 three weeks. To quantify how long it typically takes for high tracer concentrations to reach the station,
289 we computed a probability-weighted median transit time, where mean transit times were weighted by
290 their probability values. This approach ensures that frequent transport pathways are given greater
291 influence in the median transit time calculation, reducing bias from rare, low-probability trajectories.

292 2.3 Data

293 2.3.1 Biogeochemistry data

294 This study used data from the Sylt Roads long-term ecological monitoring program, focusing on a
295 subset from 2000 to 2019 to ensure consistent methodology and regular sampling. From a broad range
296 of hydrographic and biogeochemical parameters covered in the dataset, this study specifically analyzed
297 suspended particulate matter (SPM; mg/L, filtered through 0.4 µm nucleopore filters, rinsed with
298 distilled water, stored frozen, and dried at 60 °C) and chlorophyll-a (Chl-a; µg/L, filtered through GF/C
299 filters (Whatman), stored at -20 °C, and extracted using 90% acetone and analyzed

300 spectrophotometrically using the trichromatic method as described by Jeffrey and Humphrey, (1975).

301 Both parameters were measured twice weekly at a sampling depth of 1 m below the surface at two
302 primary stations: the deep station at the Lister Ley channel and the shallow station at the entrance of
303 Königshafen embayment (see Fig. 1). The full dataset is publicly available on the data portal
304 PANGAEA (<https://www.pangaea.de>) and the recent evaluation is detailed in Rick et al. (2023).

305 To analyze seasonal variability, we defined the seasons based on observed cycles in Chl-a
306 concentrations at the study site, rather than calendar or astronomical definitions. Specifically, we used:
307 - winter (November 20 – February 19, low biological activity, low Chl-a);

Deleted: way

Deleted: The iterative release process was designed to capture the full range of tidal conditions and the complexity of hydrodynamic transport within the basin, ensuring that the results are statistically robust.

Deleted: (

Deleted:)

Deleted: ¶

316 - spring (February 20 – May 31, phytoplankton bloom initiation and peak);
317 - summer (June 1 – September 19, post-bloom conditions, high light, reduced Chl-a);
318 - autumn (September 20 – November 20, transitional period).

319 2.3.2 Meteorological data

320 For the statistical analysis, we also downloaded the quality checked historical meteorological data for
321 station 3032, List auf Sylt, from Climate Data Center (CDC) of the Deutscher Wetterdienst (DWD).
322 The data includes hourly mean wind speed and wind direction (dataset ID: urn:x-
323 wmo:md:de:dwd-cdc::obsgermany-climate-hourly-wind), and daily sunshine duration (dataset ID:
324 urn:wmo:md:de:dwd-cdc::obsgermany-climate-daily-kl).

325 2.3.3 Sea Surface Height data

326 Using the validated model setup (Fofonova et al., 2019; Konyssova et al., 2025), the sea surface height
327 (SSH) data were reconstructed for the deep and shallow stations. In particular, the amplitudes and
328 phases of the 15 harmonics mentioned above were obtained from the modeling output using Fast
329 Fourier Transform analysis. Subsequently, the SSH signal was reconstructed for the exact timestamps
330 of the LTER sampling using the tide package (Pawlowicz et al., 2002). This allowed us to estimate
331 the tidal elevation and phase (through the SSH and SSH gradients) at the time of sampling, which were
332 then included as input features in the statistical and neural network (NN) analyses. Their relationship is
333 illustrated and discussed in Supplementary Material, Figs. S3–S4.

334 Table 1. The physical and hydrochemical parameters used in the study (short name, units, frequency, and source)

Data	Unit	Frequency	Source
SPM	mg/L	twice weekly	Sylt Roads Marine Observatory
Chl-a	µg/L	twice weekly	Sylt Roads Marine Observatory
Wind speed and direction	m/s, degrees	hourly mean	Deutscher Wetterdienst
Light	hours	daily	Deutscher Wetterdienst
SSH	m	every 5 minutes	Model reconstruction using 13 harmonics from tpx09 and verified with the tidal gauges

335 2.4 Neural Network

336 To assess the relative contribution of biotic conditions to SPM concentrations, we employed a forward
337 NN to predict SPM based on environmental input parameters. The approach relies primarily on long-
338 term observational data, thereby enhancing the robustness of the results, complemented by model-
339 derived SSH and its temporal gradient data. Although numerical simulations are also powerful tools in
340 this context, any discrepancies they produce can largely be attributed to the choice of numerical
341 methods or the spatial and temporal resolution applied. An NN is particularly well-suited for this task,
342 as it effectively captures complex, non-linear relationships between influencing factors. We conducted

Deleted: This product was available for download from https://opendata.dwd.de/climate_environment/, last access: 28 February 2025.

Deleted: elevation

Deleted: was

Deleted: precisely for the observational time

Deleted: . The classical harmonic analysis routines from

Deleted: were utilized

Deleted: The SSH data is then used to determine the tidal phases and elevation gradients when taking samples to include in the statistical and neural network (NN) analyses

Deleted: solely

Deleted: which adds

Deleted: to

several sensitivity experiments (not shown), varying both the network depth and the number of neurons per layer. For the current application, increasing the network depth further did not improve performance.

For the first part of the experiment, the primary regression task involved predicting SPM concentrations during the winter season, which is characterized by low biological activity, as indicated by minimal Chl-a concentrations. Focusing on winter allows for a clearer assessment of physical (abiotic) drivers, such as wind forcing, with reduced biological confounding. The input features, 19 in total, of the NN model include wind magnitude at the time of sampling and averages over a series of prior time intervals (6 to 240 hours, corresponding to the intervals analyzed in Subsection 3.2.2), dominant wind direction over 6 and 12 hours (even though the correlation analysis shows only a minor impact, the non-linear effects of wind direction may still be present), salinity, SSH, and the temporal gradient of SSH (computed using a forward scheme). The results of the winter model are presented in Section 3.3.1.

To extend the analysis across seasons, we applied the same model architecture to the full dataset, initially using the same input features as in the winter setup (results in Section 3.3.3), and subsequently incorporating two additional features: temperature and the weekly sum of sunshine hours before the measurement date (21 features in total, Section 3.3.4). The latter serve as a pragmatic proxy for both Chl-a concentration and benthic algae abundance. While we do not attempt to separate these mechanisms individually, this approach is exploratory and intended to approximate their combined influence on seasonal SPM variability.

The technical details of the NN architecture are provided in the Supplementary Material, together with the complete predictor list in Table S2.

3 Results

Figure 2 presents the time series of SPM concentrations at the deep and shallow stations in the Sylt-Rømø Bight from 2000 to 2019, based on data from the Sylt Roads monitoring program (Section 2.3.1; station locations shown in Fig. 1). Both stations display a pronounced seasonal cycle, with SPM concentrations typically peaking in winter and declining during summer. The deep station shows more frequent and sustained seasonal peaks in SPM concentrations throughout the time series, whereas the shallow station tends to exhibit higher concentrations during peak events. It is also important to note that the regular sampling at the shallow station was discontinued after 2013 following the replacement of the research vessel, resulting in reduced data coverage in subsequent years.

Deleted: The NN was implemented in several steps using a feedforward architecture with three hidden layers (e.g., Jain et al., 1996), consisting of 100, 40, and 20 neurons, respectively. Each neuron acts as a simple processing unit that transforms input into output using a mathematical function. In this case, we used a hyperbolic tangent (tanh) sigmoid transfer function, which maps input values into the range between -1 and 1 and enables the model to capture complex, non-linear relationships between environmental inputs and SPM concentrations. The output layer employed a linear activation function. The Levenberg-Marquardt algorithm is used as the learning function. For training, 60% of arbitrarily chosen SPM measurements were used, while the remaining data were split for validation and testing. A separate NN was developed for each station, and the datasets for different stations were not combined.

Deleted: 21

Deleted: s

Deleted: current elevation

Deleted: elevation

Deleted: To explore seasonal dynamics more comprehensively, we extended the model to include data from all seasons, first using the same input parameters as in the winter model

Deleted: then

Deleted: prior to

Deleted: s

Moved up [3]: In the shallow coastal systems, light can reach the seafloor, stimulating benthic algae growth, provided water clarity allows sufficient light penetration (Loebl et al., 2007).

Moved up [2]: In addition, temperature affects top-down controls such as zooplankton grazing, which alters SPM composition by consuming phytoplankton and restructuring organic aggregates.

Deleted: This, in turn, helps stabilize sediments and reduce resuspension. Temperature plays a crucial role in regulating biological activity, including phytoplankton growth, bacterial metabolism, and production of extracellular polymeric substances (EPS). EPS, secreted by microorganisms, enhances particle aggregation by increasing stickiness and acting as a binding agent for fine sediments. Warmer temperatures also accelerate the decomposition of organic matter, influencing the availability of organic detritus that contributes to flocculation.

Deleted: In this study,

Deleted: but instead aim to highlight

Deleted: levels

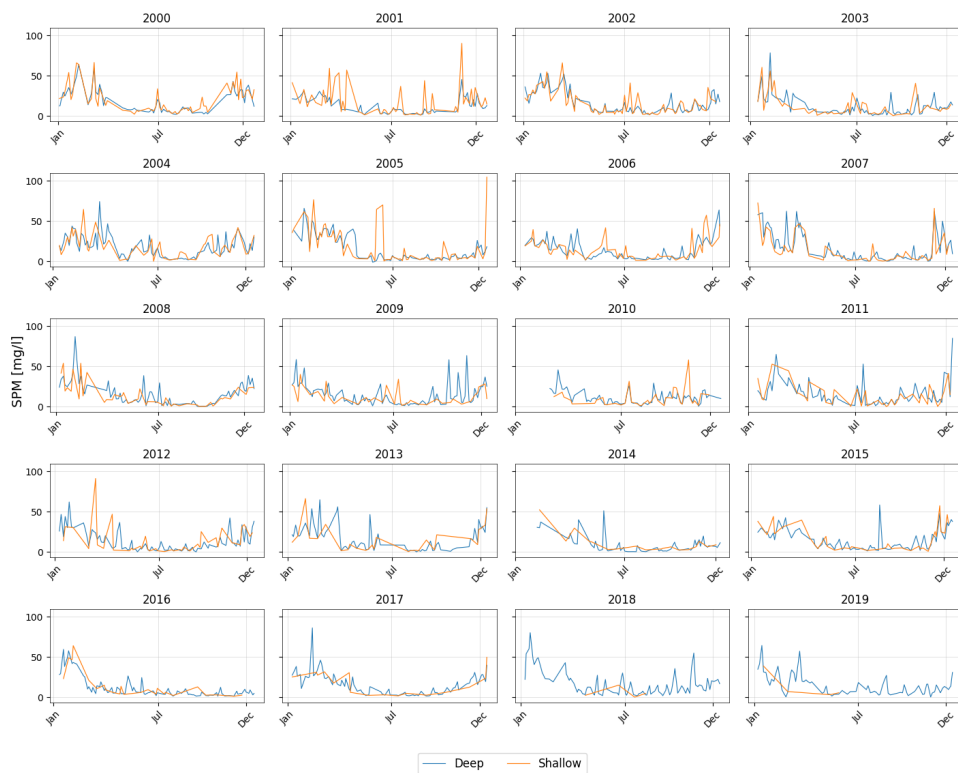
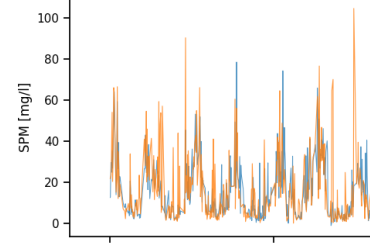


Figure 2: Time series of SPM for the considered years (2000–2019) for the deep (blue) and shallow stations (orange) gridded per year. Each subplot represents a calendar year with time on the x-axis and SPM concentration [mg/l] on the y-axis.

3.1 Seasonality of SPM concentrations

SPM concentrations show an apparent seasonality, which is further investigated in relation to biological activity and meteorological drivers in the subsequent analyses. Using Chl-a as a proxy for phytoplankton biomass, this subsection applies statistical analysis to examine how biological activity and wind forcing together shape seasonal patterns of SPM variability at both the deep and shallow stations.



Deleted:

Deleted: clear

Deleted: with patterns reflecting the combined influence of

Moved up [4]: Phytoplankton blooms in spring and summer can promote flocculation, leading to enhanced particle settling and reduced SPM concentrations in the water column (de Jonge & van Beusekom, 1995; Schartau et al., 2019).

Deleted: forcing

Deleted: While various biological processes influence SPM dynamics, phytoplankton activity plays a particularly central role by triggering biologically mediated processes and directly contributing to flocculation and particle aggregation. Phytoplankton blooms in spring and summer can promote flocculation, leading to enhanced particle settling and reduced SPM concentrations in the water column (de Jonge & van Beusekom, 1995; Schartau et al., 2019). In contrast, stronger winds during winter enhance sediment resuspension, resulting in elevated SPM levels during the colder months.

Deleted: s

3.1.1 Role of biological processes in seasonal SPM variations

Both stations exhibit distinct seasonal variations in SPM and Chl-a concentrations (Fig. 3). SPM concentrations are highest in late autumn and winter, with median values of about ~28 mg/L (33.9 ± 18.2 mg/L) at the deep and median of ~26 mg/L (38.6 ± 16.4 mg/L) at the shallow stations. In January, the peak reaches over 60 mg/L at both stations, with individual events exceeding 70 mg/L. The decline in concentrations is observed from February to May, reaching their lowest values in June to August (around 2-3 mg/L), although occasional peaks above 30-40 mg/L still occur. From September onward, SPM begins to increase. This pattern is similar at both stations, though the shallow station generally has slightly higher SPM concentrations, suggesting potential differences in sediment availability or resuspension dynamics. Chlorophyll-a concentrations follow an inverse seasonal pattern. It remains low in December-January with a median around 2 µg/L (2.1 ± 0.7 µg/L) at both stations. It increases sharply in early spring, with peaks in March-April exceeding 30 µg/L at the deep station and 25 µg/L at the shallow station. Concentrations then drop in summer, followed by a secondary increase in August-October, when values up to ~15-20 µg/L are observed.

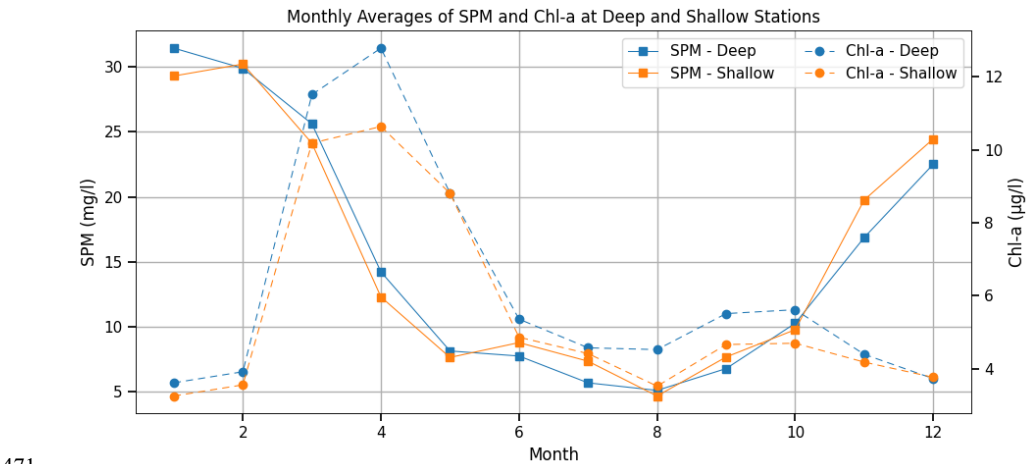


Figure 3: Monthly averages of SPM and Chl-a at the deep (blue) and shallow (orange) stations for the considered years (2000–2019). SPM concentrations (solid line with square marker, left axis) and Chl-a concentrations (dashed line with circle markers, right axis) are displayed separately for clarity. The x-axis represents the months from January to December.

The relationship between Chl-a and SPM varies across seasons (Fig. 4). During December–February, biological activity is low and Chl-a constitutes a relatively constant fraction of total SPM, both subject to the same resuspension-deposition processes. This co-settling behavior leads to strong positive correlations observed at both stations. The highest values occur at the shallow station, with $R^2 = 0.84$ in December and $R^2 = 0.75$ in January. At the deep station, correlations are relatively lower, reaching $R^2 =$

- Deleted: levels
- Deleted: on average
- Deleted: and peaking
- Deleted: i
- Deleted: at 63.5 ± 19.9 mg/L at the deep and 65.4 ± 18.3 mg/L at the shallow stations
- Deleted: through
- Deleted: spring (
- Deleted: –
- Deleted:)
- Deleted: summer (
- Deleted: –
- Deleted:)
- Deleted: averaging 2.5 ± 2.9 mg/L at both stations
- Deleted: levels
- Deleted: Chl-a
- Deleted: winter
- Deleted: on average
- Deleted: , December–January)
- Deleted: and
- Deleted: peaking between February and April before declining into summer
- Deleted: A
- Deleted: occurs
- Deleted: autumn (
- Deleted:). The deep station shows a more pronounced Chl-a peak (32.4 ± 18.1 µg/L) in early spring compared to the shallow station (25.0 ± 20.6 µg/L), though both stations exhibit a similar overall seasonal cycle
- Deleted: , with the deep station generally having a weaker correlation than the shallow station
- Deleted: winter months (
- Deleted:)
- Deleted: when
- Deleted: ,
- Deleted: are
- Deleted: ,

0.52 in December and $R^2 = 0.56$ in January. The strong correlation and the slope are in line with the resuspension of microphytobenthos as observed in winter by de Jonge and van Beusekom (1995). From March onward, the relationship becomes more complex. As Chl-a rises rapidly during the spring bloom and SPM concentrations decline, the correlation at both stations weakens with R^2 values dropping to near-zero in March. This divergence reflects differences in vertical distribution and settling behavior. While phytoplankton is a component of SPM and both are retained on the filter, their decoupling in spring and summer may reflect that not all phytoplankton is floc-associated. Active phytoplankton may remain suspended near the surface, while denser biomineral flocs sink more rapidly, leading to weaker correlations in integrated surface samples. This non-linear and temporally variable influence of Chl-a also underlies the decision not to use it directly as a predictor in the neural network (Section 3.3), but instead to approximate biological activity through more general proxy variables such as temperature and light availability (see Table S2 in Supplementary Material). During June–August, as both the SPM and Chl-a concentrations reach low values, the correlation weakens further, with August showing almost no correlation at the shallow station. In November and December, the correlation strengthens again as the role of biological activity reduces and physical drivers become dominant again.

Deleted: with the highest values in December ($R^2 = 0.75$, shallow station) and January ($R^2 = 0.84$, deep station)

Deleted: is

Deleted: ($R^2 < 1$)

Deleted: the dual role of phytoplankton: it contributes directly to SPM, yet also promotes aggregation and settling, thereby reducing suspended material

Deleted: broader

Deleted: summer (

Deleted:)

Deleted: late autumn, particularly in

Deleted: ,

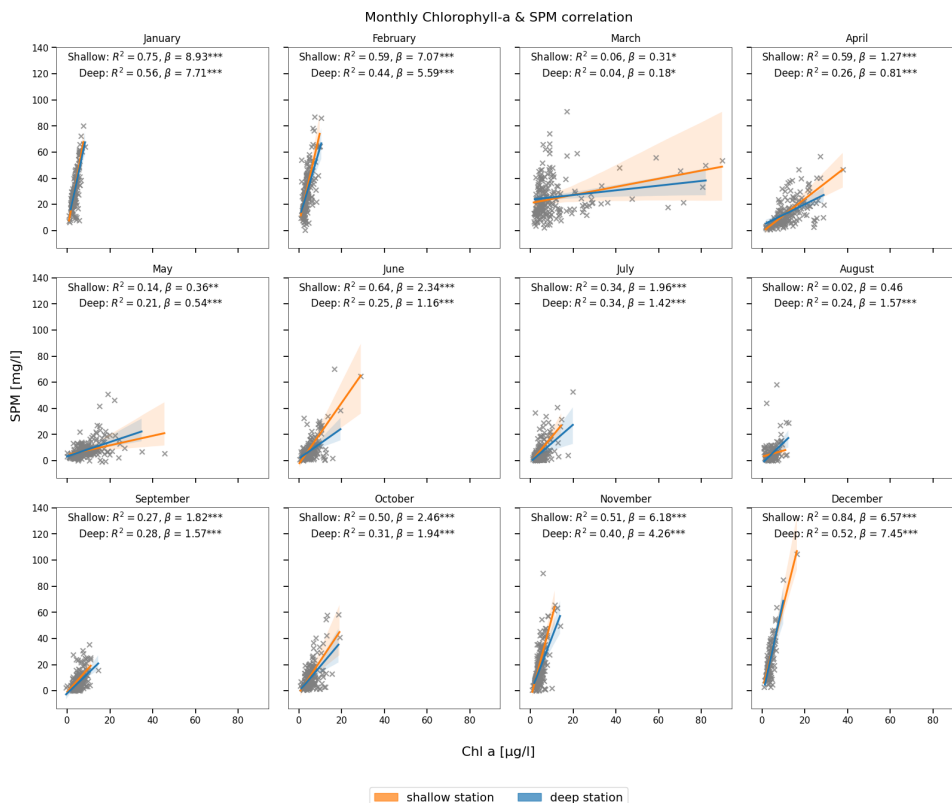


Figure 4: Monthly correlation between Chl-a (x-axis) and SPM (y-axis) concentrations at the deep (blue) and shallow (orange) stations. The coefficient of determination (R^2), slope (β), and statistical significance (* $p < 0.001$, ** $p < 0.01$, * $p < 0.05$) are indicated in each panel.**

3.1.2 Role of wind forcing in seasonal SPM variations

The relationship between seasonal SPM concentrations and wind characteristics is illustrated in Fig. 5. Wind speeds are highest in January, averaging around 8.5 ± 2.8 m/s, with peaks reaching 14.2 ± 1.7 m/s, and gradually decline through spring months, reaching a minimum with mean speeds around 6.5 ± 3.1 m/s and minima of 2.0 ± 0.7 m/s in July–August. From August onward, wind speeds begin to rise again. This seasonal cycle aligns with the observed variability in SPM, with higher concentrations in winter and lower values in summer. Dominant wind directions also vary throughout the year, with

Deleted: The results reveal a clear seasonal cycle in wind speed, which closely aligns with variations in SPM levels. The lowest wind speeds in summer correspond to the lowest SPM concentrations, while the increase in wind speeds in autumn coincides with rising SPM levels.

Deleted: winter

Deleted: in January

Deleted: . Through spring, they

Deleted: summer

Deleted: In autumn

Deleted: The dominant wind direction shifts throughout the year, with a predominance of westerly (W) and northwesterly (NW) winds, except for southerly winds in late autumn (October–November) and easterly winds in April.

westerly and northwesterly winds prevailing in most months, easterly winds in April, and more southerly winds during October–November. Seasonal wind roses illustrating these patterns are shown in the Supplementary Material (Fig. S1). However, no clear linear relationship emerges between dominant wind direction and seasonal SPM concentrations. To account for potential nonlinear interactions that may still play a role, wind direction was included as an input feature in the NN model.

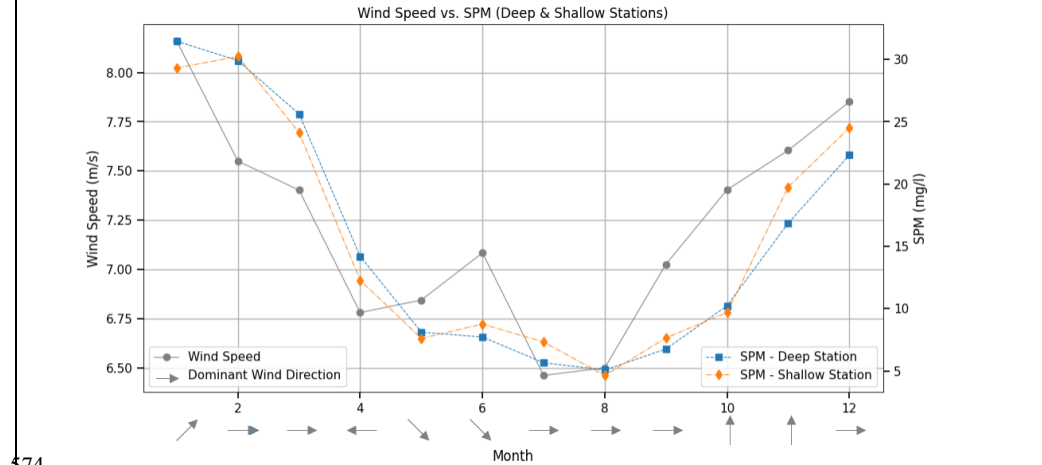


Figure 5: Monthly averages of wind speed, SPM concentrations, and dominant wind direction (2000–2019). The figure illustrates monthly mean wind speed (grey solid line, left axis) and SPM concentrations at the deep (blue squares) and shallow (orange diamonds) stations (right axis). Grey arrows along the x-axis represent the dominant wind direction for each month, with arrow orientation indicating the direction from which the wind originates, following standard meteorological convention.

While correlations are further explored in Section 3.2, the seasonal alignment of wind intensity and SPM concentrations suggests a strong physical control.

3.2 Resuspension and Time Scales of Inner Basin Transport

Beyond seasonal variation, there are mechanisms responsible for the variability of SPM concentrations on shorter temporal scales, from hours to days. This subsection examines how wind-induced resuspension operates over different time frames and the role of tidal transport within the basin.

3.2.1 Role of wind forcing in short time SPM variations

To quantify the short-term response of SPM to wind forcing, we computed Pearson correlation coefficients between SPM concentrations and wind speed averaged over different time intervals, ranging from 1 hour to 240 hours. This approach, commonly referred to as “wind memory,” allows us to evaluate how the cumulative influence of past wind conditions affects SPM variability at different depths and over varying time scales. Figure 6 illustrates how the strength of this relationship evolves as

Deleted: late autumn (Deleted:)

Deleted: ¶

Moved down [5]: The correlation between instantaneous wind speed and SPM is strongest in winter (Fig. 6), particularly pronounced at the shallow station, peaking in January with $R^2 = 0.44$. This suggests that wind-driven resuspension is a dominant control on SPM concentrations in winter. In contrast, the deep station shows much weaker correlations, with R^2 values often near zero, suggesting that the wind intensity may have a lagged effect on SPM levels. During summer (June–August), the relationship weakens significantly, with the lowest correlations observed in August for both stations. The shallow station maintains some correlation into late summer and early autumn.

Deleted: In addition to factors playing a role in seasonal SPM variability

Deleted: levels

Deleted: in

Deleted: ¶ 3.2.1 Influence of SSH¶

Deleted: 2

Deleted: The effect of wind on SPM variability is further analyzed by assessing the correlation between SPM and wind speeds averaged over different time frames – “wind memory”

Deleted: 9

wind speeds are averaged over progressively longer intervals, ranging from 1 hour to 240 hours. This approach quantifies how SPM responds to the cumulative influence of past wind conditions over varying time scales. The results show that correlation coefficients generally increase as wind memory lengthens, reaching a peak around 12-18 hours at the shallow station and 120 hours at the deep station, followed by a slight decline. Monthly variations in the correlation patterns are provided in the Supplementary Material (Fig. S2), showing that the correlation between wind speed and SPM is generally stronger in winter than in summer, with more complex patterns during transitional months such as April and November.

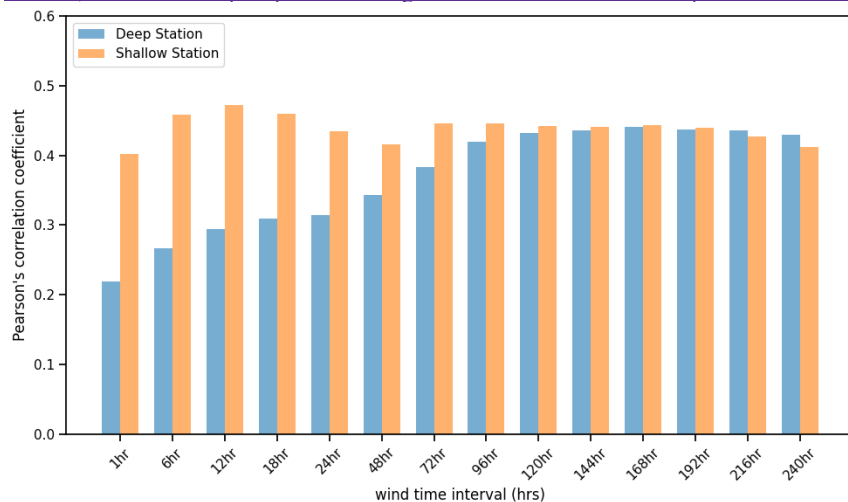


Figure 6: Pearson correlation coefficients between SPM and wind speed averaged over different time intervals, ranging from 1 hour to 240 hours. The two stations (deep station as blue and shallow station as orange) are represented separately, showing how wind memory influences SPM variability at different depths.

The correlation between instantaneous wind speed and SPM concentrations is highest in winter (Fig. 7), particularly at the shallow station, where the most substantial value occurs in January with $R^2 = 0.44$. This suggests that wind-driven resuspension may play a relatively stronger role in regulating SPM concentrations in winter. In contrast, the deep station shows much weaker correlations, with R^2 values often near zero, reflecting a lagged effect on SPM concentrations. During June–August, the relationship weakens significantly, with the lowest correlations observed in August for both stations. The shallow station maintains minor correlation ($R^2 \approx 0.15$) into late summer and early autumn.

Deleted: 9

Moved up [6]: The effect of wind on SPM variability is further analyzed by assessing the correlation between SPM and wind speeds averaged over different time frames – “wind memory”. Figure 9 illustrates how the strength of this relationship evolves as wind speeds are averaged over progressively longer intervals, ranging from 1 hour to 240 hours. This approach quantifies how SPM responds to the cumulative influence of past wind conditions over varying time scales. The results show that correlation coefficients generally increase as wind memory lengthens, reaching a peak around 12-18 hours at the shallow station and 120 hours at the deep station, followed by a slight decline.

Moved (insertion) [5]

Deleted: strongest

Deleted: 6

Deleted: pronounced

Deleted: peaking

Deleted: is a dominant control on

Deleted: suggesting that the wind intensity may have

Deleted: levels

Deleted: summer (

Deleted:)

Deleted: some

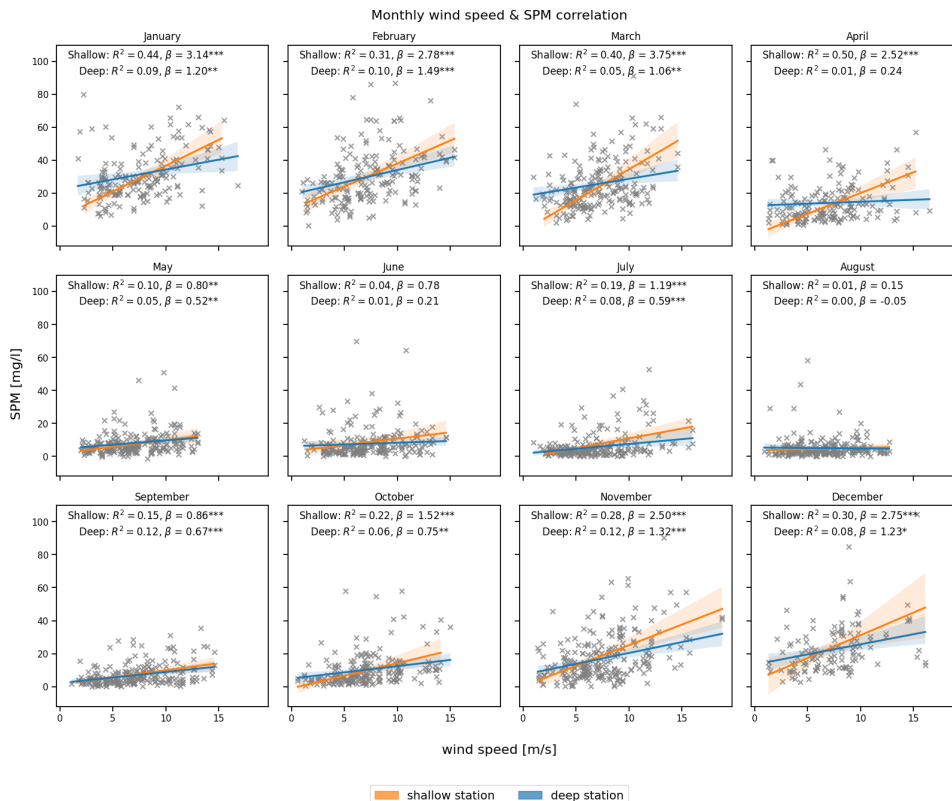


Figure 7: Monthly correlation between wind speed at the time of sampling (x-axis) and SPM concentration (y-axis) at the deep (blue) and shallow (orange) stations. The coefficient of determination (R^2), slope (β), and statistical significance (***) $p < 0.001$, ** $p < 0.01$, * $p < 0.05$) are indicated in each panel.

In contrast to the instantaneous impact of wind-speed, averaging wind speed over 120 hours (5 days) results in an improved correlation between wind and SPM at the deep station, as shown in Fig. 8, although the seasonal pattern remains similar. The stronger relationship is particularly evident in the winter and autumn months, especially at the deep station (e.g., $R^2 = 0.35$ in September, 0.24 in November and February). These findings indicate that the average wind-speed over several days have a stronger influence on SPM concentrations at the deep station than the wind at the time of sampling. The results highlight the role of wind forcing in modulating SPM concentration variability, particularly in shallow waters during winter and autumn. Naturally, the influence of wind is less pronounced in

Deleted: 6

Deleted: stronger

Deleted: 7

Deleted: characteristics

Deleted: levels

Deleted: that wind plays a crucial role in controlling

deeper waters through direct resuspension mechanisms. However, it remains significant, with a time lag possibly caused by the transport of resuspended material from shallower zones to the deep station.

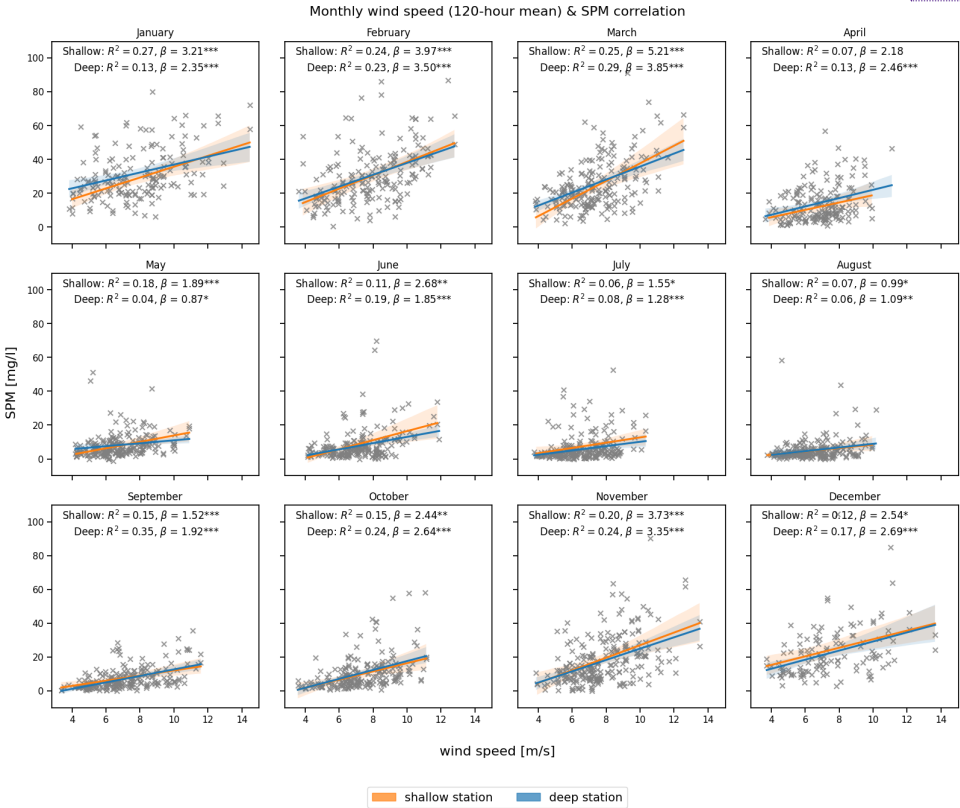


Figure 8: Monthly correlation between wind speed averaged over a 120-hour (5-day) period (x-axis) and SPM concentration (y-axis) at the deep (blue) and shallow (orange) stations. The coefficient of determination (R^2), slope (β), and statistical significance (*** $p < 0.001$, ** $p < 0.01$, * $p < 0.05$) are indicated in each panel.

Deleted: This aspect is further discussed below, in Section 3.2.3.

Deleted: 7

3.2.2 Role of tidal forcing in short time SPM variations

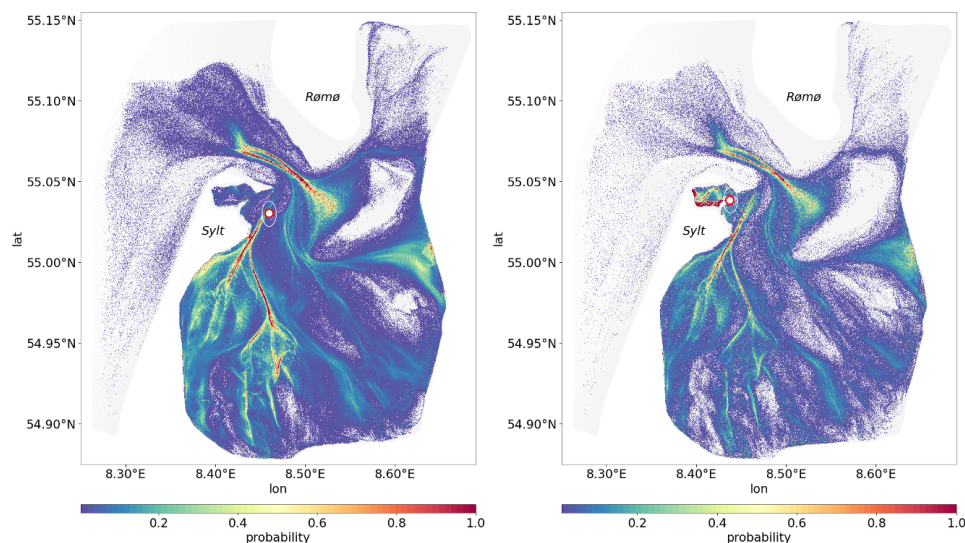


Figure 9: Probability distribution of passive tracer pathways to illustrate how frequently different areas act as source regions or transport corridors for passive tracers. Higher probability values (highlighted in yellow and red) indicate locations that more frequently contribute to SPM reaching the deep station (left panel) or shallow station (right panel).

Figure 9 shows the spatial probability distribution of passive tracer connectivity within the basin, derived from Lagrangian simulations forced solely by tides. This setup isolates the dominant physical driver of material transport in the Sylt-Rømø Bight, where tidal processes account for roughly 80% of velocity variability (Fofonova et al., 2019). While regular wind forcing (excluding storm events and uncommon multi-day episodes of strong winds from a single direction) enhances lateral dispersion, its net contribution to basin-wide transport over several days is relatively minor (Konyssova et al., 2025). Note, in this region, typical wind events last about 5–6 hours, defined as consecutive hours of wind from the same direction within an eight-sector classification (Rubinetti et al., 2023). Residual currents generated by non-linear tidal interactions establish consistent, directional transport pathways, which are effectively captured by the simulated tracer trajectories. The resulting network of tidally-induced transport pathways reveals apparent differences between the two stations. The shallow station is predominantly supplied by tracers originating in the northern parts of the bight, particularly Königshafen and its surroundings, reflecting localized and relatively rapid connections. In contrast, the deep station is influenced by broader and more distributed transport pathways, integrating material from a wider area of the basin.

Deleted: During winter, the correlation between wind speed and SPM is generally higher than in summer (Fig. 10). At the shallow station, correlation values peak within the first 12–18 hours, then slightly decline for longer wind memory intervals. This suggests that in shallow waters, the wind conditions at the time of sampling have an immediate reflection at the SPM levels. At the deep station, correlations are generally lower but gradually increase with longer wind memory intervals (~120 hours), followed by a plateau, indicating that deep-water SPM reflects rather the average wind speed for a prolonged duration before the sampling.

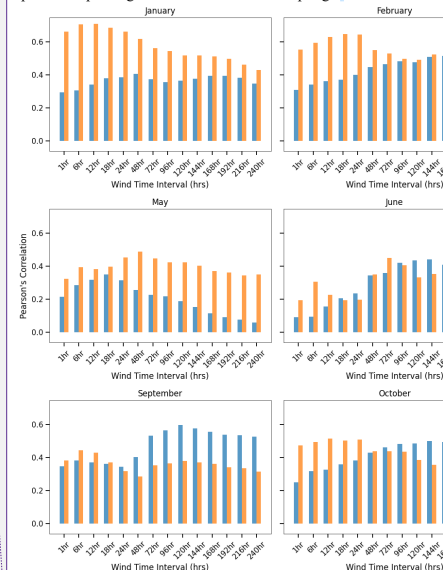


Figure 10: This figure presents the monthly variations in the correlation between wind speed and SPM across different wind memory intervals, ranging from short-term (1 hour) to long-term (360 hours).

- Deleted:** 3
- Deleted:** 11
- Deleted:** 11
- Deleted:** through vertical mixing and stochastic fluctuations
- Deleted:** tidal timescales
- Deleted:** under revision
- Deleted:** clear
- Deleted:** Each color-coded region indicates the probability of tracers originating from that area to eventually reach the deep (left) and shallow (right) stations. Tracers were removed from the simulation upon arrival, ensuring that only pre-arrival pathways are represented; tracers that failed to reach a station within the three-week tracking window were excluded. This way, the maps highlight the most frequent pathways.

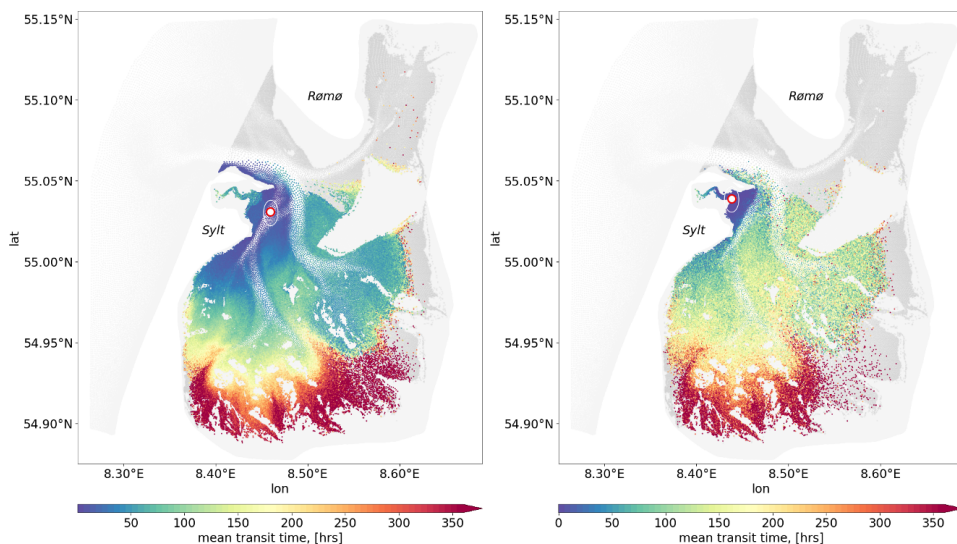


Figure 10: The mean transit time of passive tracers to reach the sampling station. The left panel corresponds to the deep station, while the right panel represents the shallow station. Grid elements that are consistently inundated with each flood phase, from which the passive tracers are released, are shown in grey. Elements that successfully reach one of the two sampling stations are colour-coded by their mean transit time (in hours), reflecting how long it takes for passive tracers to reach from a given location to each station.

For both stations, shorter transit times (depicted in blue and green, Fig. 10) are observed in areas closer to the stations, whereas regions further away, particularly in the inner tidal flats, exhibit longer transit times (yellow to red hues, Fig. 10). The transit time patterns reveal that SPM originating from intertidal areas and tidal channels follows particular pathways before reaching the deeper and shallower monitoring stations, with transport occurring on timescales of days to weeks. The difference between the two panels suggests that the deep and shallow stations receive material from primarily distinct but partially overlapping source regions.

Together, these figures illustrate the tidal connectivity of the two monitoring stations with their surrounding basin, highlighting likely source regions and typical transport pathways. To quantify the typical timescale for SPM transport, a probability-weighted transit time was computed, where individual transit times were weighted according to their interpolated probability values. This approach ensures that the estimated transit time reflects the most frequently occurring transport pathways rather than rare, low-probability trajectories. The resulting probability-weighted median transit time was 133.3 hours for the deep station, which aligns with the ~5-day wind-memory interval identified in Section 3.2.2, and 44.4 hours for the shallow station, highlighting the pronounced contrast in transport efficiency between the two locations. At the shallow station, which is situated within the Königshafen area, SPM concentrations respond to wind forcing almost immediately through local resuspension. The

Deleted: 12

Deleted: 12

Deleted: 12

Deleted: offer a comprehensive picture of SPM transport and connectivity, showing that while both stations are influenced by tidal-driven transport, they receive material from different dominant pathways. The transit time and probability maps reveal clear differences in transport dynamics between the two sampling stations. While both stations are connected to tidal-driven transport pathways, the shallow station receives material more rapidly and from more localized sources, whereas the deep station is influenced by a broader, more distributed transport network

longer transit time therefore does not indicate a delayed response, but rather reflects the additional supply of tracers arriving from a wider surrounding area, which extends the median transit time beyond the short wind-driven response captured in the memory analysis. In contrast, the deep station integrates SPM from more complex, multi-step transport routes over longer timescales. These transit times provide a key reference for interpreting observed SPM fluctuations at each station and may help distinguish between short-term and cumulative drivers of SPM variability.

3.3 Neural Network

3.3.1 Winter SPM prediction (Baseline Model)

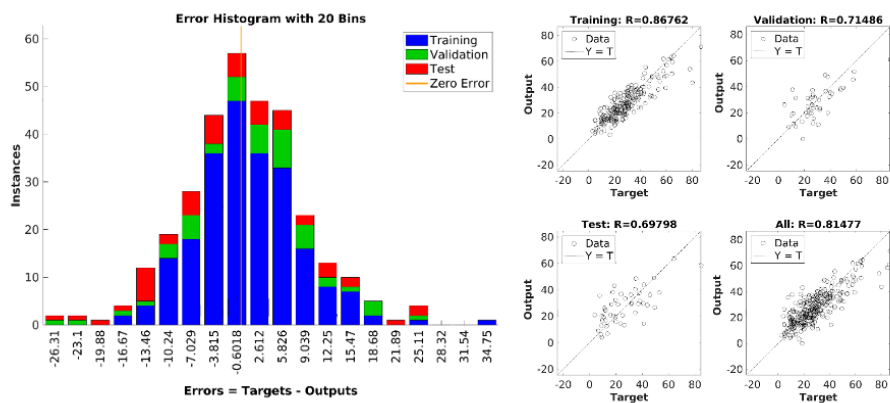


Figure 11: Performance of the neural network (NN) trained on the winter dataset for the deep station. Left: Error histogram showing the distribution of prediction errors (in mg/L) for training, validation, and test subsets. Right: Regression plots comparing predicted vs. observed SPM values, with correlation coefficients (R) for each data subset. Due to the overall qualitative similarity between the pictures for deep and shallow stations, only the deep station is presented here.

To evaluate how well physical drivers alone can explain SPM concentration variability, we first trained a baseline NN using only the winter dataset, when biological activity is minimal. This provides a reference to assess the contribution of wind and tidal forcing under conditions with limited biological influence.

The error for training, validation and testing has a normal distribution (Fig. 11, left). For the deep station, the root mean square error (RMSE), a measure of average prediction error magnitude, is 9.4 mg/L for the testing set. Note that the observed mean and median SPM concentrations in winter are 27.6 and 25.9 mg/L respectively. As a result of the application of NN to the winter dataset, they are 27.2 and 25.5 mg/L respectively (Table 2). Regression analysis (Fig. 11, right) yields correlation coefficients between observed and simulated SPMs equal to ~0.87, ~0.71, ~0.7 and ~0.81 for training, validation, testing and all winter datasets, respectively.

Deleted: Because the shallow station is located within the potential resuspension zone, this transit time does not necessarily imply a delayed response to wind forcing. Instead, it reflects the arrival of tracers from a wider surrounding area, which slightly extends the median transit time compared to what is seen in the wind memory analysis. At the same time, the relatively short overall transit time still indicates the close proximity of the primary source region, the Königshafen embayment

Deleted: 13

Deleted: 13

Deleted: levels

Deleted: ,

Deleted: a

Deleted: 13

900 The results show that, by using tidal and wind forcing along with a proxy for baroclinic conditions
901 (salinity), we can predict SPM concentrations during winter quite well without accounting for other
902 factors.
903 Notably, temperature, salinity, turbulent kinetic energy, and SPM concentrations themselves all
904 influence flocculation processes, even without considering biological activity. Temperature was
905 excluded from the feature set at this stage due to its strong seasonal cycle and its potential use as a
906 proxy for biological conditions. Specifically, in our current approach, we cannot separate the influence
907 of temperature on biological mechanisms from its physical effects (e.g. viscosity), which also impact
908 flocculation.

Deleted: levels

Moved down [16]: Next, we applied the NN trained under winter conditions to other seasons. This approach is justified by the fact that the long-term dataset captures a representative range of wind conditions in both winter and summer, including calm periods and strong wind events. Furthermore, salinity remains relatively stable across seasons, supporting the applicability of the model.

Deleted: levels

Deleted: s

909 3.3.2 Applying of NN trained on winter data to other seasons

910 Next, we applied the NN trained under winter conditions to other seasons. This approach is justified by
911 the fact that the long-term dataset captures a representative range of wind conditions in both winter and
912 summer, including calm periods and strong wind events. Furthermore, salinity remains relatively stable
913 across seasons, supporting the applicability of the model. Using the trained winter model, we attempt to
914 predict SPM concentrations for spring, summer, and autumn. The goal of this step is to estimate the
915 influence of biological processes on SPM concentrations.
916 For both stations, the results of the NN application show significantly higher SPM concentrations
917 compared to observations (Table 2).

Moved (insertion) [16]

Deleted: levels

918 Table 2. Mean, median values and correlation (R) of SPM concentrations, [mg/L], from observations VS predictions by NN
919 trained on winter dataset for the deep and shallow stations

seasons		Deep Station		Shallow Station	
		observed	predicted	observed	predicted
winter	mean, [mg/L]	27.6	27.2	28.5	24.7
	median, [mg/L]	25.9	25.5	24.4	26.5
		$R = 0.81$		$R = 0.81$	
spring	mean, [mg/L]	16.5	24.8	15.6	20.6
	median, [mg/L]	13.3	24.3	11.3	18.0
		$R = 0.29$		$R = 0.5$	
summer	mean, [mg/L]	6.15	17.7	6.8	18.5
	median, [mg/L]	4.22	16.9	3.9	16.1
		$R = 0.04$		$R = 0.35$	
autumn	mean, [mg/L]	11.6	23.4	12.8	24.0
	median, [mg/L]	8.5	22.7	7.5	21.0
		$R = 0.44$		$R = 0.54$	

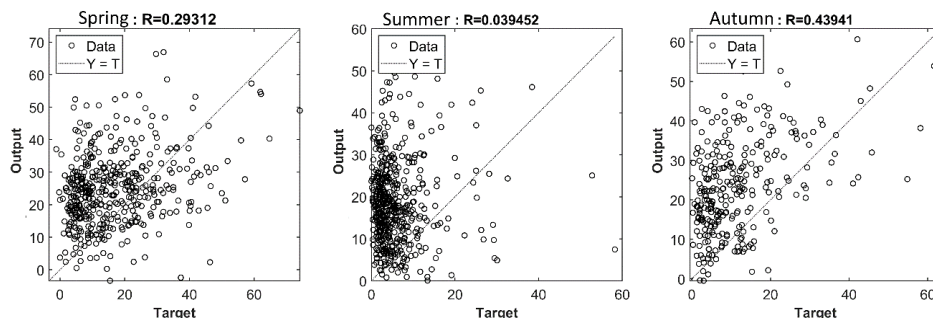


Figure 12: Regression analysis for NN trained on winter data and applied to spring, summer and autumn data vs observations. Results shown for the deep station; shallow station results are qualitatively similar and summarized in Table 2.

This discrepancy suggests that while calmer wind conditions alone can explain approximately 40% of the SPM reduction in summer compared to winter, they do not account for the full ~80% decrease observed in the data (see Table 2). The overestimation of SPM by the NN is clearly visible in the regression plots (Fig. 12), where most of the predicted values are positioned above the $Y = T$ line, particularly during summer and autumn. This does not necessarily imply that biological activity is weaker in spring, but rather that its impact is less well captured by the abiotic-only model, as biological processes contribute more strongly to variability than in autumn. The higher correlation between simulated and observed SPM in autumn likely reflects physical conditions that are more similar to winter, when the model was trained, including generally stronger winds (Section 3.2.2). In spring, enhanced biological activity and aggregation introduce variability that the model cannot account for, reducing correlation. During summer, biological processes become the primary driver of SPM concentration variability, as evidenced by the regression coefficient dropping below 0.05 (Fig. 12).

3.3.3 NN trained at the data from all seasons

Previously we showed that there are factors, in particular biological processes, which significantly influence the SPM dynamics. To confirm this, we trained NN on all the dataset (not limited to winter) using the same input features representing only abiotic conditions, which we used in 3.3.1. As expected, the overall RMSE increases to approximately 11 mg/L, due to the omission of important features that influence SPM dynamics during the warm season (Supplementary Fig. S5). When the model is trained on data from all seasons, and applied specifically to winter conditions, it underestimates SPM concentrations. For the deep station, the predicted mean and median are 19.17 mg/L and 17.2 mg/L, respectively, compared to observed values of 27.6 mg/L and 25.9 mg/L. At the shallow station, the model yields mean and median predictions of 20 mg/L and 17 mg/L, whereas the corresponding observed values are 28.45 mg/L and 24.35 mg/L. The regression coefficients also reflect this underperformance, with values of approximately $R \approx 0.66$ (deep) and 0.72 (shallow). The seasonal regression analysis further highlights these biases (Supplementary Fig. S7, upper row). A complete numerical breakdown of observed and predicted seasonal values is provided in Table S3.

Deleted: 14

Deleted: 14

Deleted: visible due to the stronger wind conditions in spring compared to summer and autumn. The correlation coefficient between simulated and observed SPM levels in autumn is much higher than in spring, which speaks to the relatively large role of biological processes in spring compared to autumn

Deleted: dynamics

Deleted: 14

Deleted: only on the

Deleted: dataset

Deleted: 21

Deleted: the model is

Deleted: for the deep station

Deleted: for the shallow station

3.3.4 Neural network trained on all-season data including biological proxy features

Including temperature and sunshine duration as proxies for biological activity improved overall model skill, reducing the test RMSE to ~ 10 mg/L. The regression analysis shows the correlation coefficient between observed and simulated SPM concentrations reached ~ 0.88 , ~ 0.76 , ~ 0.72 and ~ 0.84 for training, validation, testing and all datasets respectively (Supplementary Fig. S6). Seasonal regression plots also show marked improvements (Supplementary Fig. S7, lower row). For winter, R increased from 0.66 to 0.73 at the deep station and from 0.72 to 0.82 at the shallow station. The largest gains occurred in spring and summer, consistent with more substantial biological influence during these seasons. Table S3 provides the detailed seasonal comparison of observed and predicted means, medians, and correlations.

4 Discussion

This study set out to investigate the combined influence of wind forcing, tidal transport, and biological processes on SPM concentration variability in the Sylt-Rømø Bight. Using 20-year period monitoring data and applying statistical tools, neural network models, and Lagrangian simulations, we analyze the relative roles of these processes across seasonal and short-term timescales. In this chapter, we will further discuss topics that have not yet been fully addressed: the peculiarities of the Chl-a and SPM concentration relationship, biological processes that directly or indirectly influence SPM dynamics, further details on wind and tide control including SSH and SPM concentration relationship, details of NN related findings and study limitations.

4.1 Biological Interaction

The strong positive correlation between Chl-a and SPM concentrations in winter suggests that under low biological activity, such as limited phytoplankton growth, behaviour of both variables is driven mainly by physical processes such as wind-driven resuspension. This is consistent with previous observations in the Wadden Sea and German Bight (van Beusekom et al., 1999; van Beusekom and de Jonge, 2002). Together with SPM, the strong winds resuspend microphytobenthos attached to sediment particles (de Jonge and van Beusekom, 1995), consistent with observations by Hommersom et al. (2009), who found strong correlations between SPM and Chl-a in the Wadden Sea driven by resuspension. Such patterns support the interpretation that, under winter conditions with low biological production, a large fraction of Chl-a is contained within resuspended flocs, leading to the high correlations observed in our study at both stations. In contrast, the correlation between Chl-a and SPM concentrations begin to decline in spring, despite persistent wind forcing, and reaches a minimum in summer. This seasonal decoupling suggests that biological aggregation processes become increasingly dominant with the beginning of and following phytoplankton bloom, promoting the formation and subsequent rapid settling of flocs (Schartau et al., 2019; Maerz et al., 2016; Lunau et al., 2006). For example, the production of TEPs, secreted by phytoplankton and bacteria under certain physiological or nutrient conditions, strongly enhance particle stickiness and promote the aggregation of both organic and mineral particles (Passow, 2002). While our statistical analysis (however, not NN related efforts)

Deleted: NN trained at the data from all seasons and includes features that serve as proxies for biological processes

Deleted: The error for training, validation and testing has a normal distribution. The RMSE for the testing is

Deleted: levels

Deleted: equal to

Deleted: Supporting figures showing the error distribution and regression performance are provided in the Supplementary Material.

Deleted: Notably, adding proxies for biological processes as additional features significantly improves the overall performance of the NN trained on the full dataset. When applying this enhanced NN to winter data, the correlation coefficient increases to 0.73 at the deep station and up to 0.82 at the shallow station as opposed to 0.66 and 0.72, respectively, when input features included only abiotic factors.

Deleted: quantify

Deleted: the roles

Deleted: , wind-driven resuspension

Deleted: mediated by phytoplankton (e.g., direct contribution of phytoplankton biomass to

Deleted: , biologically induced flocculation, and trophic interactions such as grazing) to SPM variability in the Sylt-Rømø Bight. Our analysis integrates long-term in-situ observations from the Sylt Roads monitoring program and Lagrangian transport analyses based on high-resolution tidal simulations using FESOM-C

Deleted: The results reveal that SPM dynamics in this tidally energetic, well-mixed basin are governed by a complex interplay of physical and biological drivers that vary spatially and across different time scales.

The patterns of SPM variability in the Sylt-Rømø Bight are not unique to this system but reflect more general principles of ecosystem dynamics in shallow coastal environments. Similar to other parts of the Wadden Sea, this system shows a strong seasonal cycle in SPM, with winter resuspension and summer stabilization driven by a combination of wind, tidal, and biological processes (e.g., Philippart et al., 2013). Our seasonal analysis confirmed that SPM concentrations show a pronounced seasonal cycle, with high values in winter and a decline during spring and summer. Meanwhile, Chl-a concentrations, which are used as a proxy for the phytoplankton biomass, follow an inverse seasonal pattern – low in winter and peaking during early spring. Worth noting is that this study takes Chl-a concentrations as a proxy for the phytoplankton biomass, which plays a central role in initiating biologically mediated processes, including flocculation, microbial activity and grazing

Deleted: both parameters are

Deleted: largely

Deleted: (

Deleted: ,

Deleted: ,

Deleted: s

Deleted: following the phytoplankton bloom

uses Chl-a as a proxy for biological activity, it is worth noting that TEP production responds to additional drivers such as nutrient status and species composition, which can modulate flocculation potential even at similar Chl-a levels. In addition to the biological feedback, the increase in water temperature during summer also accelerates particle sinking rates by reducing water viscosity, further promoting sediment deposition (Maerz and Wirtz, 2009). This supports the view that the Chl-a–SPM relationship reflects an interplay of multiple biological and physical controls rather than a single, direct pathway. While both spring and autumn are characterized by peaks in Chl-a concentration, their influence on SPM dynamics appears to differ. In spring, calmer conditions favor particle aggregation and settling, often leading to reduced SPM levels. In autumn, however, the secondary bloom coincides with a seasonal increase in wind speed (Fig. 5), resulting in elevated SPM concentrations despite high biological activity. This suggests that enhanced organic matter availability in autumn may promote flocculation, but stronger resuspension prevents effective settling. These seasonal contrasts highlight that biological influence on SPM is strongly modulated by concurrent physical forcing. In parallel, benthic microbial processes such as biofilm formation by microphytobenthos enhance sediment stability and reduce its susceptibility to resuspension, thereby modulating the amount of SPM remaining in the water column (Andersen, 2000; Stal, 2010). Beyond microbial stabilization, benthic fauna also influences SPM dynamics through benthic-pelagic coupling. Filter-feeding benthos, such as bivalves, consume suspended particulate organic carbon (POC), effectively removing material from the water column and altering vertical fluxes of organic matter. In the Sylt-Rømø Bight, food web modelling by Baird et al. (2004) estimated that benthic consumers remove approximately 56.7 mgC m⁻² d⁻¹ of suspended POC – potentially a substantial fraction of total SPM, depending on the proportion of organic material within it. Benthic consumption likely constitutes a significant sink for fine, organic-rich particles, particularly in areas with dense benthic communities, as filter feeders remove SPM primarily through ingestion and the production of faecal pellets, which promote deposition of organic-rich material to seabed. Although the proportion of POC within SPM is known to depend on total SPM concentration (Schartau et al., 2019), robust SPM-to-POC conversion factors remain uncertain due to the unknown share of freshly formed organic matter. Although the effects of native species on benthic-pelagic coupling have been relatively well studied in the region (Baird et al., 2007), the role of introduced species remains less clear. For example, the introduction and spread of alien species such as the American razor clam (*Ensis leei*) may further amplify benthic filtration effects. In the Dutch Wadden Sea, they have shown to significantly alter trophic carbon flows, increasing carbon consumption by secondary producers and redirecting energy flows away from higher trophic levels (Jung et al., 2020). Although the abundance of *E. leei* in the Sylt-Rømø Bight has not yet been quantified, its potential influence on observed SPM concentrations provides a basis for further investigation as part of long-term ecological changes in the region.

4.2 Wind & Tide Control

The results suggest that the intensity of winds, rather than their dominant directions, exerts a stronger influence on the seasonal cycle of SPM. The seasonal patterns of wind speed, with maximum values in winter and minima in summer, aligns closely with the observed SPM concentrations, suggesting a

Deleted: t's also worth noting that, i

Deleted: While

Deleted: , benthic consumption likely constitutes a significant sink for fine, organic-rich particles, particularly in areas with dense benthic communities

Deleted: constrained

Deleted: , whose abundance in the Sylt-Rømø Bight has not yet been quantified,

Deleted: *E. leei* has been

Deleted: The hypothesis on the role of wind forcing in controlling SPM variability is supported by our further analysis.

physically mediated control during high-energy periods. During summer, the weaker relationship between wind speed and SPM concentrations points to the increasing importance of biological contribution. These may include enhanced flocculation and settling of particles, increased filtration by benthic organisms, reduced sediment availability due to biological stabilization, and overall calmer wind conditions.


Notably, correlations between wind speed and SPM are stronger at the shallow station compared to the deep station, as soon as the shallow environments are more susceptible to wind-induced turbulence. It should be noted that, since the study addresses observations of SPM concentrations, wind-induced resuspension is considered to include the effects of wave action.

In addition, the area around the shallow station is characterized by relatively small depths. Therefore, at the shallow station, the short wind-memory intervals (12–18 hours) yield the strongest correlations. Lagrangian simulations support this interpretation by illustrating that the shallow station, located within the intertidal zone itself, receives SPM directly from resuspension at the site. While these simulations do not represent full sediment dynamics, they effectively illustrate dominant source areas and transport timescales. This relatively short response time aligns with earlier observations in tidal flat systems, where wind effects on SPM are immediate in intertidal zones but take longer to become apparent in deeper areas (de Jonge and van Beusekom, 1995).

In contrast, the situation at the deep station is more complex. In addition to the larger distance between the observation point and the sea bottom, sediment characteristics in the channels are predominantly sandy, which typically requires stronger wind energy to be resuspended as opposed to the mud and finer material found in intertidal areas (Bartholomä et al., 2009). The delayed response seen in the wind memory analysis (~120 hours) and the tidally modulated transport pathways from our Lagrangian simulations (median transit time ~133 hours) likely reflects the combined influence of episodic wind-driven resuspension in shallow areas and subsequent advective transport to the deeper station (Friedrichs and Perry, 2001; de Jonge and van Beusekom, 1995). Similar multi-day lags in SPM response have been observed in other estuarine systems where tidally dominated transport pathways act on resuspended sediments originating from more energetic, nearshore zones (see also Winterwerp, 2001). Together, these results highlight a clear contrast between the two stations: rapid, localized sediment response in the shallow embayment versus slower, more integrated transport processes at the relatively deep channel.

The Lagrangian tracer simulations provide additional spatial context, revealing weak connectivity between the north-eastern and southern sections of the Sylt-Rømø Bight under regular tidal conditions. Passive tracers released in the north-eastern region rarely reach either of the sampling stations. This indicates that the stations, while valuable for long-term monitoring, may not fully capture the spatial variability of SPM dynamics across the entire basin, especially on shorter time scales.

Beyond local wind and tidal resuspension and transport within the Sylt-Rømø Bight, tidal phases also influence SPM concentrations. Naturally, higher SPM concentrations are associated with lower water levels under otherwise equal conditions, as the measurements are always taken at the surface (Fig. S3). Due to the large role of nonlinear processes in the area there is also an asymmetry between flood and ebb in terms of duration as well as mean and maximum velocities.

- Deleted:** closely mirror the trends in SPM concentrations
- Deleted:** lower
- Deleted:** activity
- Deleted:** reinforcing the notion that
- Deleted:** sensitive
- Deleted:** , while the effect at the deep station is observable with a certain delay.
- Deleted:** Our analysis of wind and tidal forcing also reveals a distinction in SPM dynamics between the shallow and deep stations.
- Deleted:** At the shallow station, SPM levels closely reflect immediate wind forcing, as evidenced by the strong correlations found over short wind memory intervals (12–18 hours). This is likely due to the limited water depth, where wind-induced turbulence can quickly mobilize sediments and elevate SPM concentrations. Additionally, given the shallowness of the area around the station, immediate resuspension in the vicinity of the station further reinforces this local signal
- Deleted:** transport
- Deleted:** further
- Deleted:** , though an important nuance should be clarified. For consistency, we applied the same analysis approach at both stations, however,
- Deleted:** is itself
- Deleted:** and
- Deleted:** The probability-weighted median transit time of about 44 hours reflects contributions from tracers released both within the Königshafen embayment, which is a primary source region, and partially from other shallow areas. While this integrated signal results in a longer median time, the actual SPM response to wind forcing at the shallow station can be nearly immediate, often occurring within one to two tidal cycles, as indicated by the short wind memory correlations.
- Deleted:** scale underscores the responsiveness of this station to local wind-driven processes and
- Deleted:** Importantly
- Deleted:** at the deep station
- Deleted:** (
- Deleted:** Given these differences, our transit time calculation ... [4]
- Moved down [17]:** 
- Deleted:** The spatial probability maps derived from Lagrang ... [5]
- Deleted:** , both of which are located in the southern basin
- Deleted:** As a result
- Deleted:** ,
- Moved (insertion) [17]**
- Deleted:** may
- Deleted:** through broader estuarine exchange processes
- Deleted:** This mechanism has been described for the Dutch ... [6]

1230 4.3 Neural Network findings

1231 The NN experiments provide a line of evidence supporting the seasonal shift in dominant SPM drivers
1232 independent of the statistical analysis. When trained only on winter data, where biological activity is
1233 minimal, the NN successfully captured winter SPM concentrations using solely physical drivers such as
1234 wind conditions within different time intervals, salinity, and tidal elevation (through SSH and SSH
1235 gradient). At both stations, this winter model performed well ($R \approx 0.81$), confirming that physical
1236 processes alone can account for most of the observed variability during this season. This reinforces the
1237 view that winter dynamics are dominated by abiotic drivers.
1238 However, when the same winter-trained model was applied to other seasons, it consistently
1239 overestimated SPM concentrations, especially in summer when biological activity is high and wind
1240 speed is generally weaker. For example, at the deep station, the observed mean SPM concentration
1241 decreased by ~78%, whereas the model reproduced only a ~36% reduction, meaning that less than half
1242 of the observed seasonal decline could be explained by abiotic factors. Similarly, at the shallow station,
1243 observed SPM declined by 80%, while the model captured only a ~42% reduction, accounting for just
1244 over half of the change. These mismatches underscore the increasing importance of biological drivers
1245 during the summer months. Interestingly, although both stations showed similar magnitudes of
1246 overestimation, the shallow station retained higher predictive skill ($R \approx 0.35$) than the deep station ($R \approx$
1247 0.04) in summer. This difference likely reflects the stronger and more immediate influence of wind
1248 forcing at the shallow site, where even in summer, intermittent wind events can rapidly mobilize
1249 sediments.
1250 The addition of biologically relevant features such as temperature and sunshine duration into the full-
1251 year NN model, in Section 3.3.4, significantly improved its performance, especially at the shallow
1252 station. While we do not explicitly resolve individual biological pathways, these proxies likely capture
1253 their cumulative effects as seen from the improved model fit indicating their aggregate influence is both
1254 detectable and substantial. These processes may include phytoplankton-driven aggregation and
1255 flocculation, microbial stabilization, and benthic-pelagic interactions such as benthic filtration. Our
1256 interpretation remains exploratory rather than conclusive, as targeted biological data would be required
1257 to quantify these mechanisms in detail.

1258 4.4 Study Limitations

1259 Although, in this study, we discuss the main driving mechanisms of SPM concentrations in the Sylt-
1260 Rømø Bight, we also acknowledge that the system is far more complex and has more factors
1261 influencing the fluctuations of SPM concentrations than we investigate here. Moreover, the SPM itself
1262 is a parameter that is composed of various components and sizes in nature, and such a level of detail is
1263 not readily available in the dataset. Incorporating measurements of sediment composition (organic
1264 versus inorganic fractions) and their sizes would add more certainty into the roles of considered
1265 mechanisms modifying SPM concentrations.
1266 Our Lagrangian transport simulations use massless passive tracers, which do not account
1267 for flocculation, deposition, or resuspension processes. Incorporating such processes would require a
1268 different modeling framework and additional data that are not currently available, including detailed

Deleted: parameters

Deleted: parameters

Deleted: reasonably

Deleted: is

Deleted: levels

Deleted: ¶

Deleted: A

Deleted: from 27.6 mg/L in winter to 6.2 mg/L in summer

Deleted: . The winter-trained NN predicted

Deleted: (winter R increased to 0.82 as opposed to $R \approx 0.72$ when input features included only abiotic factors)

Deleted: The potential contribution of these mechanisms is discussed in more detail in Section 4.1.

Deleted: levels

Deleted: levels

Deleted: levels

Deleted: As we discussed the role of different processes, we grounded on the observed concentrations and idealised model simulations. However, the settling and resuspension processes are not directly simulated in the study.

Moved down [18]: Such processes would require a different modeling framework and more detailed data, including the more accurate habitat maps and sediment grain sizes.

Deleted: S

Deleted: more detailed data

Deleted: the more accurate

1295 habitat maps and reliable estimates of SPM fluxes from the open boundary. Nonetheless, despite these
 1296 simplifications, the model effectively captures key patterns of spatial connectivity pathways and
 1297 timescales driven by tidal dynamics.
 1298 Another limitation is that changes in the SPM input from the open boundary cannot be quantified. Net
 1299 coastward transport from the North Sea likely contributes to seasonal variability, for example, through
 1300 enhanced import or retention in spring and summer (Burchard et al., 2008; Postma, 1981), but we lack
 1301 data to resolve this numerically.
 1302 In addition, more precise SPM predictions would benefit from neural network architectures with
 1303 “memory”, such as Long Short-Term Memory (LSTM) models, which can account for the delayed
 1304 effects of biotic and abiotic conditions over several months. A North Sea-wide approach would be
 1305 required to capture these long-term dynamics and boundary-driven influences. Within such a
 1306 framework, it would also be appropriate to include additional predictors such as nutrient concentrations
 1307 and benthic processes to represent better the complex interactions driving SPM variability.
 1308 While this study does not claim to offer a comprehensive representation of all the processes in play, we
 1309 believe that our work presents new insights to understand better the baseline mechanisms of SPM
 1310 concentration variability within the basin and across multiple timescales.

1311 **5 Conclusions**

1312 This study investigated the primary drivers of SPM variability in the Sylt-Rømø Bight, a semi enclosed
 1313 basin with well-mixed conditions and hydrodynamics dominantly shaped by tides. We combined long-
 1314 term monitoring data (SPM, Chl-a, wind conditions, and light availability) with SSH reconstructed from
 1315 a validated hydrodynamic model, and applied statistical analyses and neural network modelling. In
 1316 addition, Lagrangian transport simulations were used to assess tidal connectivity and transport
 1317 timescales. Together, these approaches revealed new insights on SPM concentration variability across
 1318 multiple timescales and relative influence of the main driving mechanisms.
 1319 Our findings confirm that wind speed is the dominant driver of short-term SPM variability, particularly
 1320 at the shallow station, where SPM concentrations respond almost immediately to wind forcing. This
 1321 rapid response, especially during winter and autumn, highlights the importance of wind-driven
 1322 resuspension in shallow waters. In contrast, the deep station exhibits a more delayed response to wind
 1323 forcing, with peak correlations occurring at longer wind memory intervals (~5 days). This lag reflects
 1324 the fact that, at greater depths, direct resuspension due to immediate wind forcing plays a reduced role,
 1325 while the transport of material from neighboring shallower areas becomes increasingly important.
 1326 Tidal dynamics primarily regulate the advection processes within the basin, redistributing fine, easily
 1327 resuspendable material from shallow to the deeper areas. Lagrangian simulations illustrate that SPM at
 1328 the shallow station originates locally, predominantly from within or around the Königshafen
 1329 embayment. Meanwhile, at the deep station, SPM is likely supplied from the intertidal and shallow by
 1330 the tidally driven redistribution over a longer timescale (~133 hours), consistent with the observed
 1331 wind-memory lag (~120 hours). These results highlight the fundamental distinction between localized,
 1332 wind-driven resuspension and slower, broader-scale, tide-driven transport, both of which shape SPM
 1333 variability but at different spatial and temporal scales.

- Deleted:** sediment grain sizes
- Deleted:** . However
- Deleted:** the lack of direct
- Deleted:** However, we hypothesise that this factor does not exhibit a strong seasonal cycle.
- Deleted:** fully
- Deleted:** better
- Deleted:** better
- Deleted:** As we move forward, more holistic hydro- and morphodynamic model simulations would be an interesting step to further unravel the contribution of event-based processes (extreme heat, storm events), density-driven transport, and food-web interaction.
- Deleted:** Based on long-term time-series of environmental parameters such as SPM, Chl-a, winds and light availability, in combination with Lagrangian transport simulations and application of NN methods, the analysis revealed new insights on SPM dynamics across multiple timescales and relative influence of the main driving mechanisms
- Deleted:** Strong correlations between wind speed and SPM
- Deleted:** indicate that
- Deleted:** occurs rapidly

Seasonal analyses further emphasize the shifting balance between physical and biological controls in shaping SPM dynamics. While wind and tides dominate winter SPM variability, the onset of the spring phytoplankton bloom corresponds with a decline in SPM concentrations, likely due to biological aggregation and flocculation, leading to enhanced particle settling. The inverse seasonal patterns of Chl-
a and SPM supports this interpretation, aligning with previous studies that describe the role of phytoplankton in promoting flocculation and sedimentation in coastal systems. NN experiments suggest that calmer wind conditions alone can explain approximately ~40% of the observed summer SPM reduction compared to winter ~~concentrations~~. Still, they do not account for up to ~80% decrease seen in the data. This substantial reduction is likely influenced by a variety of biologically related mechanisms, ranging from the microbial activity, production of EPS to zooplankton grazing. Further studies are needed to quantify the relative contributions of these individual mechanisms. Overall, this study provides a comprehensive and quantitative assessment of how wind, tides, and biological activity interact to control SPM variability in a shallow, tidally dominated coastal system.

Deleted: levels
Deleted: ,
Deleted: but

Conflict of Interest

The authors declare that they have no conflict of interest.

Author Contributions

GK performed the data analysis and wrote the initial draft of the manuscript. GK, VS, and AA carried out the numerical simulations. JvB, GK, and VS conceptualized the study. SH, SR, IK, and KHW contributed to the discussion of methods and interpretation of the results. All authors contributed to manuscript review and editing.

Funding

This study has been funded by the German Federal Ministry of Education and Research (BMBF) in the frame of the joint research projects MGF-Nordsee (FKZ 03F0847A), CREATE (03F0910B) and Coastal Futures (FKZ 03F0911J) part of the research mission “Protection and Sustainable use of Marine Areas”, within the German Marine Research Alliance (DAM).

Data Availability

The source code of the FESOM-C model is publicly available via Zenodo: <https://doi.org/10.5281/zenodo.2085177> (Androsov et al., 2018). The Sylt Roads observational dataset is accessible through the PANGAEA data portal: <https://doi.org/10.1594/PANGAEA.873549>, <https://doi.org/10.1594/PANGAEA.873547>, <https://doi.org/10.1594/PANGAEA.918018>, <https://doi.org/10.1594/PANGAEA.918032>, <https://doi.org/10.1594/PANGAEA.918027>, <https://doi.org/10.1594/PANGAEA.918023>, <https://doi.org/10.1594/PANGAEA.918033>, <https://doi.org/10.1594/PANGAEA.918028>, <https://doi.org/10.1594/PANGAEA.918024>, <https://doi.org/10.1594/PANGAEA.918034>, <https://doi.org/10.1594/PANGAEA.918029>.

Deleted: <https://www.pangaea.de>.

<https://doi.org/10.1594/PANGAEA.918025>, <https://doi.org/10.1594/PANGAEA.918035>,
<https://doi.org/10.1594/PANGAEA.918030>, <https://doi.org/10.1594/PANGAEA.918026>,
<https://doi.org/10.1594/PANGAEA.918036>, and <https://doi.org/10.1594/PANGAEA.918031>.
 Meteorological data, including hourly wind characteristics (station 3032, List auf Sylt; dataset ID: *urn:x-wmo:md:de.dwd.cdc::obsgermany-climate-hourly-wind*) and daily sunshine duration (*urn:wmo:md:de-dwd-cdc:obsgermany-climate-daily-kl*), are available from the Climate Data Center (CDC) of the Deutscher Wetterdienst (DWD): https://opendata.dwd.de/climate_environment/. The Lagrangian model output and Neural Network results are available from the corresponding author upon reasonable request.

Acknowledgements

We thank the teams involved in the Sylt Roads long-term ecological monitoring program for providing essential in-situ data. We also acknowledge the Deutscher Wetterdienst (DWD) Climate Data Center for access to freely available meteorological datasets. This study was conducted as part of the research mission “Protection and Sustainable Use of Marine Areas” of the German Marine Research Alliance (DAM) and was financially supported by the German Federal Ministry of Education and Research (BMBF).

References

Aarup, T.: Transparency of the North Sea and Baltic Sea - a Secchi depth data mining study, *Oceanologia*, 44, 323–337, 2002.
 Andersen, T. J.: The role of fecal pellets in sediment settling at an intertidal mudflat, the Danish Wadden Sea, in: *Proceedings in Marine Science*, vol. 3, edited by: McAnally, W. H. and Mehta, A. J., Elsevier, 387–401, [https://doi.org/10.1016/S1568-2692\(00\)80133-3](https://doi.org/10.1016/S1568-2692(00)80133-3), 2000.
 Androsov, A., Fofonova, V., Kuznetsov, I., Danilov, S., Rakowsky, N., Harig, S., Holger, B., and Wiltshire, K.H.: FESOM-C, , <https://doi.org/10.5281/ZENODO.2085177>, 2018.
 Androsov, A., Fofonova, V., Kuznetsov, I., Danilov, S., Rakowsky, N., Harig, S., Brix, H., and Wiltshire, K. H.: FESOM-C v.2: coastal dynamics on hybrid unstructured meshes, *Geosci. Model Dev.*, 12, 1009–1028, <https://doi.org/10.5194/gmd-12-1009-2019>, 2019.
 Baird, D., Asmus, H., and Asmus, R.: Energy flow of a boreal intertidal ecosystem, the Sylt-Rømø Bight, *Mar. Ecol. Prog. Ser.*, 279, 45–61, <https://doi.org/10.3354/meps279045>, 2004.
 Baird, D., Asmus, H., and Asmus, R.: Trophic dynamics of eight intertidal communities of the Sylt-Rømø Bight ecosystem, northern Wadden Sea, *Mar. Ecol. Prog. Ser.*, 351, 25–41, <https://doi.org/10.3354/meps07137>, 2007.

1425 Bale, A., Morris, A., and Howland, R.: Seasonal sediment movement in the Tamar Estuary,
1426 Oceanologica Acta, 8, 1–6, 1985.

1427 Bartholomä, A., Kubicki, A., Badewien, T. H., and Flemming, B. W.: Suspended sediment transport in
1428 the German Wadden Sea—seasonal variations and extreme events, Ocean Dynamics, 59, 213–225,
1429 <https://doi.org/10.1007/s10236-009-0193-6>, 2009.

1430 Becherer, J., Flöser, G., Umlauf, L., and Burchard, H.: Estuarine circulation versus tidal pumping:
1431 Sediment transport in a well-mixed tidal inlet, JGR Oceans, 121, 6251–6270,
1432 <https://doi.org/10.1002/2016JC011640>, 2016.

1433 Bruns, I., Bartholomä, A., Menjua, F., and Kopf, A.: Physical impact of bottom trawling on seafloor
1434 sediments in the German North Sea, Front. Earth Sci., 11, 1233163,
1435 <https://doi.org/10.3389/feart.2023.1233163>, 2023.

1436 Burchard, H., Flöser, G., Staneva, J. V., Badewien, T. H., and Riethmüller, R.: Impact of Density
1437 Gradients on Net Sediment Transport into the Wadden Sea, Journal of Physical Oceanography, 38, 566–
1438 587, <https://doi.org/10.1175/2007JPO3796.1>, 2008.

1439 Cadée, G. C.: Increased phytoplankton primary production in the Marsdiep area (Western Dutch
1440 Wadden Sea), Netherlands Journal of Sea Research, 20, 285–290, [https://doi.org/10.1016/0077-7579\(86\)90050-5](https://doi.org/10.1016/0077-7579(86)90050-5), 1986.

1442 Christiansen, C., Vølund, G., Lund-Hansen, L. C., and Bartholdy, J.: Wind influence on tidal flat
1443 sediment dynamics: Field investigations in the Ho Bugt, Danish Wadden Sea, Marine Geology, 235,
1444 75–86, <https://doi.org/10.1016/j.margeo.2006.10.006>, 2006.

1445 Cloern, J. E.: Turbidity as a control on phytoplankton biomass and productivity in estuaries, Continental
1446 Shelf Research, 7, 1367–1381, [https://doi.org/10.1016/0278-4343\(87\)90042-2](https://doi.org/10.1016/0278-4343(87)90042-2), 1987.

1447 Colijn, F.: Light absorption in the waters of the Ems-Dollard estuary and its consequences for the
1448 growth of phytoplankton and microphytobenthos, Netherlands Journal of Sea Research, 15, 196–216,
1449 [https://doi.org/10.1016/0077-7579\(82\)90004-7](https://doi.org/10.1016/0077-7579(82)90004-7), 1982.

1450 de Jonge, V. N.: Relations Between Annual Dredging Activities, Suspended Matter Concentrations, and
1451 the Development of the Tidal Regime in the Ems Estuary, Can. J. Fish. Aquat. Sci., 40, s289–s300,
1452 <https://doi.org/10.1139/f83-290>, 1983.

1453 de Jonge, V. N. and van Beusekom, J. E. E.: Wind- and tide-induced resuspension of sediment and
1454 microphytobenthos from tidal flats in the Ems estuary, Limnol. Oceanogr., 40, 776–778,
1455 <https://doi.org/10.4319/lo.1995.40.4.0776>, 1995.

Moved (insertion) [7]

Moved down [15]: Van Beusekom, J. E. E. and de Jonge, V. N.: Long-term changes in Wadden Sea nutrient cycles: importance of organic matter import from the North Sea, in: Nutrients and Eutrophication in Estuaries and Coastal Waters, edited by: Orive, E., Elliott, M., and de Jonge, V. N., Springer Netherlands, Dordrecht, 185–194, https://doi.org/10.1007/978-94-017-2464-7_15, 2002. Van Beusekom, J. E. E., Brockmann, U. H., Hesse, K.-J., Hickel, W., Poremba, K., and Tillmann, U.: The importance of sediments in the transformation and turnover of nutrients and organic matter in the Wadden Sea and German Bight, Deutsche Hydrographische Zeitschrift, 51, 245–266, <https://doi.org/10.1007/BF02764176>, 1999.

Moved (insertion) [8]

Deleted: Christiansen, C., Vølund, G., Lund-Hansen, L. C., and Bartholdy, J.: Wind influence on tidal flat sediment dynamics: Field investigations in the Ho Bugt, Danish Wadden Sea, Marine Geology, 235, 75–86, <https://doi.org/10.1016/j.margeo.2006.10.006>, 2006.

- de Jonge, V. N. and de Jong, D. J.: 'Global Change' Impact of Inter-Annual Variation in Water Discharge as a Driving Factor to Dredging and Spoil Disposal in the River Rhine System and of Turbidity in the Wadden Sea, *Estuarine, Coastal and Shelf Science*, 55, 969–991, <https://doi.org/10.1006/ecss.2002.1039>, 2002.
- Depestele, J., Ivanović, A., Degrendele, K., Esmacili, M., Polet, H., Roche, M., Summerbell, K., Teal, L. R., Vanellander, B., and O'Neill, F. G.: Measuring and assessing the physical impact of beam trawling, *ICES Journal of Marine Science*, 73, i15–i26, <https://doi.org/10.1093/icesjms/fsv056>, 2016.
- Dissanayake, D. M. P. K., Ranasinghe, R., and Roelvink, J. A.: The morphological response of large tidal inlet/basin systems to relative sea level rise, *Climatic Change*, 113, 253–276, <https://doi.org/10.1007/s10584-012-0402-z>, 2012.
- Dolch, T. and Reise, K.: Long-term displacement of intertidal seagrass and mussel beds by expanding large sandy bedforms in the northern Wadden Sea, *Journal of Sea Research*, 63, 93–101, <https://doi.org/10.1016/j.seares.2009.10.004>, 2010.
- Dronkers, J.: Tidal asymmetry and estuarine morphology, *Netherlands Journal of Sea Research*, 20, 117–131, [https://doi.org/10.1016/0077-7579\(86\)90036-0](https://doi.org/10.1016/0077-7579(86)90036-0), 1986.
- Dyer, K. R.: Chapter 14 Sediment Transport Processes in Estuaries, in: *Developments in Sedimentology*, vol. 53, Elsevier, 423–449, [https://doi.org/10.1016/S0070-4571\(05\)80034-2](https://doi.org/10.1016/S0070-4571(05)80034-2), 1995.
- Egbert, G. D. and Erofeeva, S. Y.: Efficient Inverse Modeling of Barotropic Ocean Tides, *J. Atmos. Oceanic Technol.*, 19, 183–204, [https://doi.org/10.1175/1520-0426\(2002\)019<0183:EIMOBO>2.0.CO;2](https://doi.org/10.1175/1520-0426(2002)019<0183:EIMOBO>2.0.CO;2), 2002.
- Eisma, D.: Flocculation and de-flocculation of suspended matter in estuaries, *Netherlands Journal of Sea Research*, 20, 183–199, [https://doi.org/10.1016/0077-7579\(86\)90041-4](https://doi.org/10.1016/0077-7579(86)90041-4), 1986.
- Engel, A. and Schartau, M.: Influence of transparent exopolymer particles (TEP) on sinking velocity of *Nitzschia closterium* aggregates, *Mar. Ecol. Prog. Ser.*, 182, 69–76, <https://doi.org/10.3354/meps182069>, 1999.
- Fettweis, M., Monbaliu, J., Baeye, M., Nechad, B., and van Den Eynde, D.: Weather and climate induced spatial variability of surface suspended particulate matter concentration in the North Sea and the English Channel, *Methods in Oceanography*, 3–4, 25–39, <https://doi.org/10.1016/j.mio.2012.11.001>, 2012.
- Flöser, G., Burchard, H., and Riethmüller, R.: Observational evidence for estuarine circulation in the German Wadden Sea, *Continental Shelf Research*, 31, 1633–1639, <https://doi.org/10.1016/j.csr.2011.03.014>, 2011.

Deleted: Fettweis, M. and van Den Eynde, D.: The mud deposits and the high turbidity in the Belgian–Dutch coastal zone, southern bight of the North Sea, *Continental Shelf Research*, 23, 669–691, [https://doi.org/10.1016/S0278-4343\(03\)00027-X](https://doi.org/10.1016/S0278-4343(03)00027-X), 2003.

1507 Fofonova, V., Androsov, A., Sander, L., Kuznetsov, I., Amorim, F., Hass, H. C., and Wiltshire, K. H.:
 1508 Non-linear aspects of the tidal dynamics in the Sylt-Rømø Bight, south-eastern North Sea, *Ocean Sci.*,
 1509 15, 1761–1782, <https://doi.org/10.5194/os-15-1761-2019>, 2019.

1510 Friedrichs, C. T. and Aubrey, D. G.: Non-linear tidal distortion in shallow well-mixed estuaries: a
 1511 synthesis, *Estuarine, Coastal and Shelf Science*, 27, 521–545, [https://doi.org/10.1016/0272-7714\(88\)90082-0](https://doi.org/10.1016/0272-7714(88)90082-0), 1988.

1512 Friedrichs, C. and Perry, J.: Tidal salt marsh morphodynamics: a synthesis, *Journal of Coastal Research*,
 1513 27, 7–37, 2001.

1515 Graf, G. and Rosenberg, R.: Bioresuspension and biodeposition: a review, *Journal of Marine Systems*,
 1516 11, 269–278, [https://doi.org/10.1016/S0924-7963\(96\)00126-1](https://doi.org/10.1016/S0924-7963(96)00126-1), 1997.

1517 Hagen, R., Winter, C., and Kösters, F.: Changes in tidal asymmetry in the German Wadden Sea, *Ocean
 1518 Dynamics*, 72, 325–340, <https://doi.org/10.1007/s10236-022-01509-9>, 2022.

1519 Hommersom, A., Peters, S., Wernand, M. R., and De Boer, J.: Spatial and temporal variability in bio-
 1520 optical properties of the Wadden Sea, *Estuarine, Coastal and Shelf Science*, 83, 360–370,
 1521 <https://doi.org/10.1016/j.ecss.2009.03.042>, 2009.

1522 Jansen, H., van Den Bogaart, L., Hommersom, A., and Capelle, J.: Spatio-temporal analysis of sediment
 1523 plumes formed by mussel fisheries and aquaculture in the western Wadden Sea, *Aquacult. Environ.
 1524 Interact.*, 15, 145–159, <https://doi.org/10.3354/aei00458>, 2023.

1525 Jeffrey, S. W. and Humphrey, G. F.: New spectrophotometric equations for determining chlorophylls a,
 1526 b, c1 and c2 in higher plants, algae and natural phytoplankton, *Biochemie und Physiologie der Pflanzen*,
 1527 167, 191–194, [https://doi.org/10.1016/S0015-3796\(17\)30778-3](https://doi.org/10.1016/S0015-3796(17)30778-3), 1975.

1528 Jung, A., van Der Veer, H., Philippart, C., Waser, A., Ens, B., de Jonge, V., and Schückel, U.: Impacts
 1529 of macrozoobenthic invasions on a temperate coastal food web, *Mar. Ecol. Prog. Ser.*, 653, 19–39,
 1530 <https://doi.org/10.3354/meps13499>, 2020.

1531 Konyssova, G., Sidorenko, V., Androsov, A., Sander, L., Danilov, S., Rubinetti, S., Burchard, H.,
 1532 Winter, C., Wiltshire, K.H.: Changes in tidal dynamics in response to sea level rise in the Sylt-Rømø
 1533 Bight (Wadden Sea), *Ocean Dynamics*, 75, 43, <https://doi.org/10.1007/s10236-025-01688-1>, 2025.

1534 Kuznetsov, I., Androsov, A., Fofonova, V., Danilov, S., Rakowsky, N., Harig, S., and Wiltshire, K. H.:
 1535 Evaluation and Application of Newly Designed Finite Volume Coastal Model FESOM-C, Effect of
 1536 Variable Resolution in the Southeastern North Sea, *Water*, 12, 1412,
 1537 <https://doi.org/10.3390/w12051412>, 2020.

Moved (insertion) [10]

Moved (insertion) [11]

Moved (insertion) [12]

Deleted: Jain, A. K., Jianchang Mao, and Mohiuddin, K. M.: Artificial neural networks: a tutorial, *Computer*, 29, 31–44, <https://doi.org/10.1109/2.485891>, 1996.

Deleted: V

Deleted: de Jonge, V. N.: Relations Between Annual Dredging Activities, Suspended Matter Concentrations, and the Development of the Tidal Regime in the Ems Estuary, *Can. J. Fish. Aquat. Sci.*, 40, s289–s300, <https://doi.org/10.1139/f83-290>, 1983.
de Jonge, V. N. and van Beusekom, J. E. E.: Wind- and tide-induced resuspension of sediment and microphytobenthos from tidal flats in the Ems estuary, *Limnol. Oceanogr.*, 40, 776–778, <https://doi.org/10.4319/lo.1995.40.4.0776>, 1995.

1550 Kuznetsov, I., Rabe, B., Androsov, A., Fang, Y.-C., Hoppmann, M., Quintanilla-Zurita, A., Harig, S.,
 1551 Tippenhauer, S., Schulz, K., Mohrholz, V., Fer, I., Fofonova, V., and Janout, M.: Dynamical
 1552 reconstruction of the upper-ocean state in the central Arctic during the winter period of the MOSAiC
 1553 expedition, *Ocean Sci.*, 20, 759–777, <https://doi.org/10.5194/os-20-759-2024>, 2024.

1554 Lettmann, K. A., Wolff, J.-O., and Badewien, T. H.: Modeling the impact of wind and waves on
 1555 suspended particulate matter fluxes in the East Frisian Wadden Sea (southern North Sea), *Ocean*
 1556 *Dynamics*, 59, 239–262, <https://doi.org/10.1007/s10236-009-0194-5>, 2009.

1557 Loebl, M., Dolch, T., and van Beusekom, J. E. E.: Annual dynamics of pelagic primary production and
 1558 respiration in a shallow coastal basin, *Journal of Sea Research*, 58, 269–282,
 1559 <https://doi.org/10.1016/j.seares.2007.06.003>, 2007.

1560 Lunau, M., Lemke, A., Dellwig, O., and Simon, M.: Physical and biogeochemical controls of
 1561 microaggregate dynamics in a tidally affected coastal ecosystem, *Limnol. Oceanogr.*, 51, 847–859,
 1562 <https://doi.org/10.4319/lo.2006.51.2.0847>, 2006.

1563 Maerz, J., Hofmeister, R., van Der Lee, E. M., Gräwe, U., Riethmüller, R., and Wirtz, K. W.: Maximum
 1564 sinking velocities of suspended particulate matter in a coastal transition zone, *Biogeosciences*, 13,
 1565 4863–4876, <https://doi.org/10.5194/bg-13-4863-2016>, 2016.

1566 Maerz, J. and Wirtz, K.: Resolving physically and biologically driven suspended particulate matter
 1567 dynamics in a tidal basin with a distribution-based model, *Estuarine, Coastal and Shelf Science*, 84,
 1568 128–138, <https://doi.org/10.1016/j.ecss.2009.05.015>, 2009.

1569 Neder, C., Fofonova, V., Androsov, A., Kuznetsov, I., Abele, D., Falk, U., Schloss, I. R., Sahade, R.,
 1570 and Jerosch, K.: Modelling suspended particulate matter dynamics at an Antarctic fjord impacted by
 1571 glacier melt, *Journal of Marine Systems*, 231, 103734, <https://doi.org/10.1016/j.jmarsys.2022.103734>,
 1572 2022.

1573 Pawlowicz, R., Beardsley, B., and Lentz, S.: Classical tidal harmonic analysis including error estimates
 1574 in MATLAB using T_TIDE, *Computers & Geosciences*, 28, 929–937, [https://doi.org/10.1016/S0098-3004\(02\)00013-4](https://doi.org/10.1016/S0098-3004(02)00013-4), 2002.

1576 Postma, H.: Sediment transport and sedimentation in the estuarine environment, *American Association*
 1577 *of Advanced Sciences*, 83, 158–179, 1967.

1578 Postma, H.: Exchange of materials between the North Sea and the Wadden Sea, *Marine Geology*, 40,
 1579 199–213, [https://doi.org/10.1016/0025-3227\(81\)90050-5](https://doi.org/10.1016/0025-3227(81)90050-5), 1981.

1580 Purkiani, K., Becherer, J., Flöser, G., Gräwe, U., Mohrholz, V., Schuttelaars, H. M., and Burchard, H.:
 1581 Numerical analysis of stratification and destratification processes in a tidally energetic inlet with an ebb
 1582 tidal delta, *J. Geophys. Res. Oceans*, 120, 225–243, <https://doi.org/10.1002/2014JC010325>, 2015.

Moved (insertion) [13]

Deleted: Philippart, C. J. M., Salama, Mhd. S., Kromkamp, J. C., van Der Woerd, H. J., Zuur, A. F., and Cadée, G. C.: Four decades of variability in turbidity in the western Wadden Sea as derived from corrected Secchi disk readings, *Journal of Sea Research*, 82, 67–79, <https://doi.org/10.1016/j.seares.2012.07.005>, 2013.

1588 Rick, J. J., Scharfe, M., Romanova, T., van Beusekom, J. E. E., Asmus, R., Asmus, H., Mielck, F.,
1589 Kamp, A., Sieger, R., and Wiltshire, K. H.: An evaluation of long-term physical and hydrochemical
1590 measurements at the Sylt Roads Marine Observatory (1973–2019), Wadden Sea, North Sea, Earth Syst.
1591 Sci. Data, 15, 1037–1057, <https://doi.org/10.5194/essd-15-1037-2023>, 2023.

1592 [Rubinetti, S., Fofonova, V., Arnone, E., and Wiltshire, K. H.: A Complete 60-Year Catalog of Wind](#)
1593 [Events in the German Bight \(North Sea\) Derived From ERA5 Reanalysis Data, Earth and Space](#)
1594 [Science, 10, e2023EA003020, <https://doi.org/10.1029/2023EA003020>, 2023.](#)

1595 Schartau, M., Riethmüller, R., Flöser, G., van Beusekom, J. E. E., Krasemann, H., Hofmeister, R., and
1596 Wirtz, K.: On the separation between inorganic and organic fractions of suspended matter in a marine
1597 coastal environment, Progress in Oceanography, 171, 231–250,
1598 <https://doi.org/10.1016/j.pocean.2018.12.011>, 2019.

1599 Sidorenko, V., Rubinetti, S., Akimova, A., Pogoda, B., Androsov, A., Beng, K. C., Sell, A. F., Pineda-
1600 Metz, S. E. A., Wegner, K. M., Brand, S. C., Shama, L. N. S., Wollschläger, J., Klemm, K., Rahdarian,
1601 A., Winter, C., Badewien, T., Kuznetsov, I., Herrling, G., Laakmann, S., and Wiltshire, K. H.:
1602 Connectivity and larval drift across marine protected areas in the German bight, North Sea: Necessity of
1603 stepping stones, Journal of Sea Research, 204, 102563, <https://doi.org/10.1016/j.seares.2025.102563>,
1604 2025.

1605 Sprong, P. A. A., Fofonova, V., Wiltshire, K. H., Neuhaus, S., Ludwichowski, K. U., Käse, L.,
1606 Androsov, A., and Metfies, K.: Spatial dynamics of eukaryotic microbial communities in the German
1607 Bight, Journal of Sea Research, 163, 101914, <https://doi.org/10.1016/j.seares.2020.101914>, 2020.

1608 Stal, L. J.: Microphytobenthos as a biogeomorphological force in intertidal sediment stabilization,
1609 Ecological Engineering, 36, 236–245, <https://doi.org/10.1016/j.ecoleng.2008.12.032>, 2010.

1610 [van Beusekom, J. E. E. and de Jonge, V. N.: Long-term changes in Wadden Sea nutrient cycles:](#)
1611 [importance of organic matter import from the North Sea, in: Nutrients and Eutrophication in Estuaries](#)
1612 [and Coastal Waters, edited by: Orive, E., Elliott, M., and de Jonge, V. N., Springer Netherlands,](#)
1613 [Dordrecht, 185–194, \[https://doi.org/10.1007/978-94-017-2464-7_15\]\(https://doi.org/10.1007/978-94-017-2464-7_15\), 2002.](#)

1614 [van Beusekom, J. E. E., Brockmann, U. H., Hesse, K.-J., Hickel, W., Poremba, K., and Tillmann, U.:](#)
1615 [The importance of sediments in the transformation and turnover of nutrients and organic matter in the](#)
1616 [Wadden Sea and German Bight, Deutsche Hydrographische Zeitschrift, 51, 245–266,](#)
1617 <https://doi.org/10.1007/BF02764176>, 1999.

1618 [van Maren, D. S., van Kessel, T., Cronin, K., and Sittoni, L.: The impact of channel deepening and](#)
1619 [dredging on estuarine sediment concentration, Continental Shelf Research, 95, 1–14,](#)
1620 <https://doi.org/10.1016/j.csr.2014.12.010>, 2015.

Deleted: Reise, K. and Siebert, I.: Mass occurrence of green algae in the German Wadden Sea, Deutsche Hydrographische Zeitschrift. Supplement. Hamburg[DTSCH. HYDROGR. Z.(SUPPL.)]. 1994., 1994.

Deleted: Schubel, J. R.: Gas Bubbles and the Acoustically Impenetrable, or Turbid, Character of Some Estuarine Sediments, in: Natural Gases in Marine Sediments, edited by: Kaplan, I. R., Springer US, Boston, MA, 275–298, https://doi.org/10.1007/978-1-4684-2757-8_16, 1974.

Deleted: Stanev, E. V., Schulz-Stellenfleth, J., Staneva, J., Grayek, S., Grashorn, S., Behrens, A., Koch, W., and Pein, J.: Ocean forecasting for the German Bight: from regional to coastal scales, Ocean Sci., 12, 1105–1136, <https://doi.org/10.5194/os-12-1105-2016>, 2016.

Deleted: V

Deleted: V

Deleted: V

Verney, R., Lafite, R., and Brun-Cottan, J.-C.: Flocculation Potential of Estuarine Particles: The Importance of Environmental Factors and of the Spatial and Seasonal Variability of Suspended Particulate Matter, *Estuaries and Coasts*, 32, 678–693, <https://doi.org/10.1007/s12237-009-9160-1>, 2009.

Winterwerp, J. C.: Stratification effects by cohesive and noncohesive sediment, *J. Geophys. Res.*, 106, 22559–22574, <https://doi.org/10.1029/2000JC000435>, 2001.

Wotton, R.: The Essential Role of Exopolymers (Eps) in Aquatic Systems, in: *Oceanography and Marine Biology*, vol. 20042243, edited by: Gibson, R., Atkinson, R., and Gordon, J., CRC Press, 57–94, <https://doi.org/10.1201/9780203507810.ch3>, 2004.

Moved (insertion) [14]

Moved up [7]: Bartholomä, A., Kubicki, A., Badewien, T. H., and Suspended sediment transport in the German Wadden Sea—seasonal variations and extreme events, *Ocean Dynamics*, 59, 213–225, <https://doi.org/10.1007/s10236-009-0193-6>, 2009.

Bruns, I., Bartholomä, A., Menjua, F., and Kopf, A.: Physical impact of bottom trawling on seafloor sediments in the German North Sea, *Front. Earth Sci.*, 11, 1233163, <https://doi.org/10.3389/feart.2023.1233163>, 2023.

Christiansen, C., Vølund, G., Lund-Hansen, L. C., and Bartholdy, J.: Wind influence on tidal flat sediment dynamics: Field investigations in the Ho Bugt, Danish Wadden Sea, *Marine Geology*, 235, 75–86, <https://doi.org/10.1016/j.margeo.2006.10.006>, 2006.

De Jonge, V. N. and De Jong, D. J.: ‘Global Change’ Impact of Inter-Annual Variation in Water Discharge as a Driving Factor to Dredging and Spoil Disposal in the River Rhine System and of Turbidity in the Wadden Sea, *Estuarine, Coastal and Shelf Science*, 55, 969–991, <https://doi.org/10.1006/ecss.2002.1039>, 2002.

Moved up [8]: Bruns, I., Bartholomä, A., Menjua, F., and Kopf, of bottom trawling on seafloor sediments in the German North Sea, *Front. Earth Sci.*, 11, 1233163, <https://doi.org/10.3389/feart.2023.1233163>, 2023.

Christiansen, C., Vølund, G., Lund-Hansen, L. C., and Bartholdy, J.:

Moved up [9]: Christiansen, C., Vølund, G., Lund-Hansen, L. C., Wind influence on tidal flat sediment dynamics: Field investigations in the Ho Bugt, Danish Wadden Sea, *Marine Geology*, 235, 75–86, <https://doi.org/10.1016/j.margeo.2006.10.006>, 2006.

De Jonge, V. N. and De Jong, D. J.: ‘Global Change’ Impact of Inter-

Moved up [10]: Friedrichs, C. and Perry, J.: Tidal salt marsh synthesis, *Journal of Coastal Research*, 27, 7–37, 2001.

Hommersom, A., Peters, S., Wernand, M. R., and De Boer, J.: Spatial and temporal variability in bio-optical properties of the Wadden Sea, *Estuarine, Coastal and Shelf Science*, 83, 360–370,

Moved up [11]: Hommersom, A., Peters, S., Wernand, M. R., and temporal variability in bio-optical properties of the Wadden Sea, *Estuarine, Coastal and Shelf Science*, 83, 360–370, <https://doi.org/10.1016/j.ecss.2009.03.042>, 2009.

Jansen, H., Van Den Bogaart, L., Hommersom, A., and Capelle, J.:

Moved up [12]: Jansen, H., Van Den Bogaart, L., Hommersom, Spatio-temporal analysis of sediment plumes formed by mussel fisheries and aquaculture in the western Wadden Sea, *Aquacult. Environ. Interact.*, 15, 145–159, <https://doi.org/10.3354/aei00458>, 2023.

Moved up [13]: Lettmann, K. A., Wolff, J.-O., and Badewien, T. impact of wind and waves on suspended particulate matter fluxes in the East Frisian Wadden Sea (southern North Sea), *Ocean Dynamics*, 59, 239–262, <https://doi.org/10.1007/s10236-009-0194-5>, 2009.

Van Maren, D. S., Van Kessel, T., Cronin, K., and Sittoni, L.: The

Moved up [14]: Verney, R., Lafite, R., and Brun-Cottan, J.-C.: of Estuarine Particles: The Importance of Environmental Factors and of the Spatial and Seasonal Variability of Suspended Particulate Matter, *Estuaries and Coasts*, 32, 678–693, <https://doi.org/10.1007/s12237-009-9160-1>, 2009.

Deleted: Bartholomä, A., Kubicki, A., Badewien, T. H., and Flemming, B. W.: Suspended sediment transport in the German Wadden Sea—seasonal variations and extreme events, *Ocean Dynamics*, 59, 213–225, <https://doi.org/10.1007/s10236-009-0193-6>, 2009.

... [7]

▼

Page 14: [1] Deleted	Gaziza Konyssova	7/14/25 8:47:00 AM
----------------------	------------------	--------------------

▼

Page 18: [2] Deleted	Gaziza Konyssova	7/31/25 6:38:00 PM
----------------------	------------------	--------------------

▼

Page 18: [3] Deleted	Gaziza Konyssova	7/14/25 10:16:00 AM
----------------------	------------------	---------------------

▼

Page 25: [4] Deleted	Gaziza Konyssova	8/6/25 4:52:00 PM
----------------------	------------------	-------------------

▼

Page 25: [5] Deleted	Gaziza Konyssova	8/6/25 10:42:00 PM
----------------------	------------------	--------------------

▼

Page 25: [6] Deleted	Gaziza Konyssova	9/12/25 4:01:00 PM
----------------------	------------------	--------------------

▼

Page 35: [7] Deleted	Gaziza Konyssova	9/19/25 4:36:00 PM
----------------------	------------------	--------------------

▼